WILEY-VCH

Core/Shell Metal Halide Perovskite Nanocrystals for Optoelectronic Applications

Chengxi Zhang, Jiayi Chen, Lingmei Kong, Lin Wang, Sheng Wang, Wei Chen, Rundong Mao, Lyudmila Turyanska, Guohua Jia* and Xuyong Yang*

Dr. C. Zhang, L. Kong, Dr. L. Wang, Dr. S. Wang, Prof. X. Yang

Key Laboratory of Advanced Display and System Applications of Ministry of Education, Shanghai University, 149 Yanchang Road, Shanghai 200072, P. R. China

E-mail: yangxy@shu.edu.cn

J. Chen, Dr. W. Chen, R. Mao, Dr. G. Jia

Curtin Institute of Functional Molecules and Interfaces, School of Molecular and Life Sciences, Curtin University, GPO Box U1987, WA 6845, Australia

E-mail: guohua.jia@curtin.edu.au

Dr. L. Turyanska

Faculty of Engineering, University of Nottingham, Nottingham, NG7 2RD, UK

Abstract

Core/shell structured metal halide perovskite nanocrystals (NCs) are emerging as a type of materials with remarkable optical and electronic properties. Research into this field has been developing and expanding rapidly in recent years, with significant advances in the studies of the shell growth mechanism and in understanding of properties of these materials. Significant enhancement of both the stability and the optical performance of core/shell perovskite NCs is of particular importance for their applications in optoelectronic technologies. In this review, we summarize the recent advances in core/shell structured perovskite NCs. We elaborate the band structures and configurations of core/shell perovskite NCs, review the shell classification and shell engineering approaches, such as perovskites and their derivative shells, semiconductor shell, oxide shell, polymer shell and discuss the shell growth mechanisms. The prospective of these NCs in lighting and displays, solar cells, photodetectors and other devices is discussed in the light of current knowledge, remaining challenges and future opportunities.

Keywords: metal halide perovskites, core/shell nanocrystals, shell growth mechanisms, optical properties, optoelectronics

1. Introduction

In recent years, halide perovskite nanocrystals (NCs) have attracted significant attention in both fundamental research and industrial applications, owing to their excellent optical and electronic properties including tunable emission across the ultraviolet (UV)-visible spectral range, high extinction coefficient, narrow luminescence line width, high photoluminescence quantum yield (PLQY) and high defect tolerance.[1-4] These intrinsic properties make them promising candidates for a wide range of applications, such as light-emitting diodes (LEDs),[5-7] lasers,[8, 9] photodetectors,[10] biological probes,[11] solar cells,[12] and photocatalysis.[13] In particular, their remarkable optoelectronic performances render them a possible game-changer.

To date, the most extensively investigated perovskite organic-inorganic halide perovskite NCs have a formula of ABX_3, where A is methylammonium (MA, $CH_3NH_3^+$) or formamidinium (FA, $CH(NH_2)_2^+$), B is Pb^{2+} or Sn^{2+}, and X is Cl^-, Br^-, I^- or mixture of them.[14] However, the issues of their intrinsic thermal instability and easy-degradation, when they are exposed to oxygen and/or humidity, need to be addressed to improve their environmental stability and shelf life.[15, 16] Replacing MA or FA in the organic-inorganic halide perovskite NCs with Cs^+ was shown to produce all-inorganic perovskites with enhanced stability.[17-19] Moreover, various capping ligands, such as iminodibenzoic acid (IDA), trioctylphosphine oxide (TOPO) and didodecyldimethylammonium bromide (DDAB), were also explored in an attempt to improve perovskite NC stability.[6, 19-21] However, the soft ionic nature of all-inorganic halide perovskites also may result in the decomposition or degradation of such materials when exposing to polar solvents, light, heat and oxygen, and can lead to phase transitions, hence posing substantial challenges for the practical applications of halide perovskite NCs.

For conventional semiconductor NCs, synthesis of core/shell heterostructures has been well established and widely used to tailor their optical and electronic properties, and thus to enhance their stability.[22-27] The capabilities of a shell layer in effectively passivating the

surface traps of semiconductor NCs and improving their performance in optoelectronic devices have been demonstrated.[28, 29] Similarly, overgrowth of a shell on top of the core of perovskite NCs could provide a powerful strategy to improve their stability. Although the trap states in perovskite NCs are known to be within the valence band/conduction band or to form shallow defect states, the improvement of the formation of core/shell structures can endow perovskite NCs with new properties, such as enhanced electron/hole separation and transfer, which are beneficial for their application in photovoltaic devices and catalysis.[30-33] Despite recent extensive research efforts being devoted to conducting the growth of core/shell perovskite NCs, consolidated understanding and strategies are yet to be established.

In this review, we present a summary of the recent advances on the growth of core/shell perovskite NCs aiming to improve their stability and therefore enhance their optoelectronic performance. The compositions and categories of the shell materials are discussed, and the effect of shell is explained using band structures of the obtained core/shell heterostructures. Particular attention is focused on the lattice mismatch, which dominates the epitaxial growth of the core/shell heterostructures. Synthetic strategies for growth of core/shell structured perovskites including *in-situ* synthesis, post-synthesis overgrowth and shell engineering are discussed. We summarize the advances in the growth of these structures based on the shell material type and the NC architecture, i.e., core/shell perovskites are classified into groups based on shell material: semiconductor shell, oxide shell, polymer shell. The improvement in NC stability and optoelectronic properties achieved for core/shell structures is systematically considered with respect to their potential applications in lighting and displays, solar cells, photodetectors, etc. The review gives insight into the core/shell structure of perovskite NCs, summarizing the remaining challenges and proposing future outlook.

2. Band structures and configurations of core/shell perovskite nanocrystals

Optical properties of perovskite NCs can be tuned by their compositions and size/shape in a wide range of electromagnetic spectrum, from the UV to the near-infrared ranges, making them promising candidates for many applications.[34-36] To improve the stability and the optoelectronic performance, the overgrowth of the original NCs with a shell is proposed as a promising strategy. Research into development of growth strategies and studies of the properties of these core/shell structured perovskite NCs have attracted considerable attention in recent years. In this section, classification, band structures, lattice mismatch between dissimilar materials of core-shell perovskite NCs are discussed. Defect tolerance, which is one of the inherent features of perovskite materials, is also elaborated.

2.1 Architectures of core/shell perovskite nanocrystals

Figure 1 Schematic illustration of core/shell architectures, including **a)** $CsPbBr_3/Cs_4PbBr_6$ core/shell structure. Reproduced with permission.[37] Copyright 2018, RSC. **b)** $CsPbBr_3/SiO_2$ modified by 2-methoxyethanol. Reproduced with permission.[38] Copyright 2017, Wiley-VCH. **c)** $CsPbX_3$/MPMs/SiO_2 hybrid microspheres. Reproduced with permission.[39] Copyright 2019, Wiley-VCH.

A number of shell growth strategies for perovskite NCs have emerged in recent years, producing a variety of core/shell architectures. These strategies include overgrowth of an individual perovskite NC with a shell of another material, embedding multiple perovskite NCs into a shell matrix, coating perovskite NCs with multiple shells, decorating or modifying the surfaces of perovskite NCs with shell-like NCs, etc. (**Figure 1**).[37-40] *In-situ* and post-synthesis

strategies have been used to achieve these architectures and the majority of these studies adopt an epitaxial growth approach for the core/shell perovskite NC growth. As shown in Figure 1a, Li group synthesized $CsPbBr_3/Cs_4PbBr_6$ core/shell structures by a seeded growth method, in which the pre-synthesized $CsPbBr_3$ seeds were coated with Cs_4PbBr_6 in the presence of halide and cesium precursors.[37] The PLQY of the obtained core/shell structures reached 96.2%, which is higher than that of the initial seeds (85%). A layer of shell material can separate perovskite NCs from each other, and thus can improve their photostability by suppressing the re-growth of perovskite NCs induced by light illumination. Zhang *et al.*[41] reported an epitaxial growth strategy to prepare stable core/alloyed-shell/shell $FAPbBr_3/FA_xCs_{1-x}PbBr_3/CsPbBr_3$ NCs. The formation of an intermediate alloyed layer of $FA_xCs_{1-x}PbBr_3$ in these core/shell structures alleviates the lattice mismatch between the core and the shell, thus resulting in the ternary structured NCs with a high PLQY of 93%.

In another widely used approach, silica or polymers are employed as the shell materials to construct micron-sized core/shell structures with embedded multiple NCs (Figure 1b). The chemically inert and optically transparent silica coating can improve the NC stability while maintaining optical properties of embedded perovskite NCs. Also, polymers can modify the surface functionalities of the perovskite NCs, making them suitable for specific applications such as biomedical applications.[11, 42, 43] Hu *et al.*[38] prepared $CsPbBr_3/SiO_2$ NCs through a waterless *in-situ* growth method, in which multiple perovskite NCs were embedded into a silica sphere. The formation of a SiO_2 layer improves stability of $CsPbBr_3$ NCs against humility while the multiple light-scattering intensity between $CsPbBr_3$ NCs results in 50% decrease of the amplified spontaneous emission (ASE) threshold and 388% increase of the relative light-output efficiency.

Wang *et al.*[42] developed a spray-assisted transition process to encapsulate $CsPbBr_3$ perovskite NCs into poly(methyl methacrylate) (PMMA) polymer nanospheres, forming

$CsPbBr_3$/PMMA globules suitable for live-cell imaging. In addition, mesoporous polystyrene microspheres (MPMs) were used by Yang *et al.*[39] to load $CsPbBr_3$ NCs before coating this composite structure with a layer of SiO_2 to produce $CsPbBr_3$/MPMs/SiO_2 multi-core/shell structures (Figure 1c). The obtained MPMs have low thermal conductivity, good hydrophobicity, acid and alkaline resistance, and can provide numerous anchor sites for large-volume perovskite NCs loading. The silica shell was used to seal the pores of the MPMs to prevent leakage of the perovskite NCs, and the long alkyl chains also can passivate the surfaces of MPMs and improve the solvent resistance. Other multilayer structures are also reported. For example, Xu *et al.*[44] prepared double shell-protected $CsPbBr_3$/Cs_4PbBr_6/SiO_2 composites by evenly encapsulating $CsPbBr_3$/Cs_4PbBr_6 NCs into the silica matrix after these NCs were synthesized through a precipitation process. In these structures, the Cs_4PbBr_6 provides moisture and heat resistance, and silica matrix provides further protection and enables NC dispersion in organic binders for their application in inks. The perovskite NCs embedded into multi-shell composites have several benefits, such as good fluorescence properties, environmental stability and new unique functionalities. It is worth noting that during the growth of double shells, size increase of the perovskite NCs may occur, especially for those NCs coated with organic shells.

2.2 Band structures of core/shell perovskite nanocrystals

2.2.1 Definition of type I and type II core/shell structures

Before the shell growth of perovskite NCs, the shell materials are carefully selected for the design of core/shell structures to allow favorable band alignment. In a type I core/shell structure, the shell material has a wider energy bandgap than the core, and hence the conduction band and the valence band edges of the core material are located inside the energy gap of shell, leading to that the electrons and holes are localized within the core. The bandgap of the core material determines the bandgap energy of this heterostructure, while the shell provides

passivation of the surface defects and confines the electrons and holes within the core. This could improve the overall optical properties and stability of the NCs.[28, 29] A number of type I perovskite structures were successfully demonstrated, including $CsPbBr_3/Cs_4PbBr_6$,[45] $CsPbBr_3/Rb_4PbBr_6$,[46] $CsPbBr_3/CdS$,[47] etc.

The type II structures have a staggered band alignment where the edges of valence and conduction band of the core material are at lower or higher energies than those of the shell material. The bandgap of a type II structure is determined by the energy separation between the edge of conduction band of one semiconductor and the edge of the valence band of the other semiconductor. The carriers are spatially separated in these structures, hence offering potential benefits for applications in photovoltaics and photocatalysis, etc.,[29, 48] as was demonstrated with core/shell NCs, such as $CsPbBr_3/TiO_2$,[49] $CsPbBr_3$/zeolitic[50] and $CsPbI_3/ZrO_2$.[51]

2.2.2 Band structures of core/shell perovskite nanocrystals

For each core material, the band structures of core/shell perovskite NCs can be modified by the shell material used, producing either type I or type II core/shell structures, and can be tailored for specific applications.

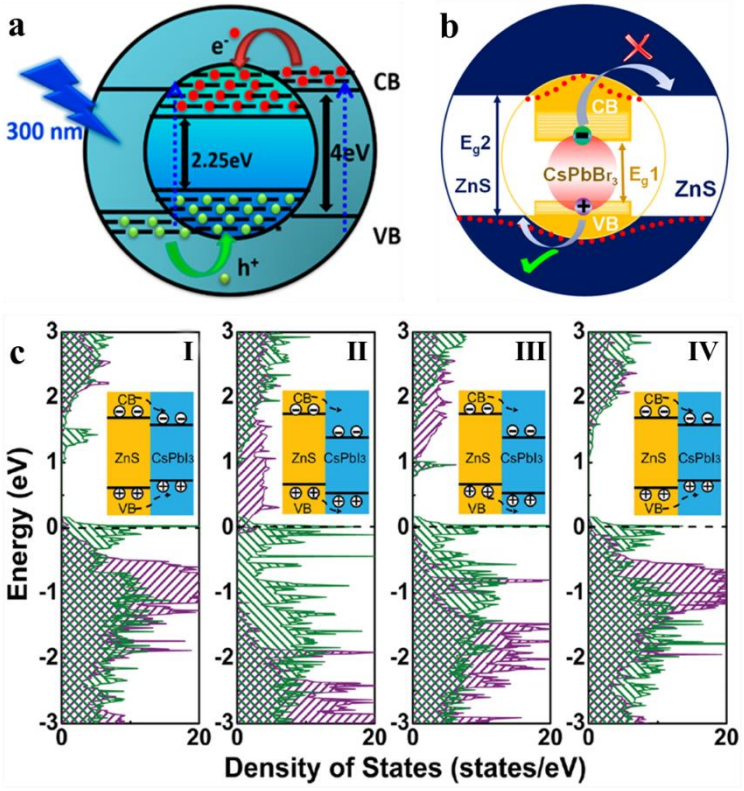

Figure 2 Schematic diagram of band energy alignment in **a)** $CsPbBr_3/Cs_4PbBr_6$ NCs. Reproduced with permission.[52] Copyright 2019, ACS. **b)** Pseudo type-II $CsPbBr_3$/ZnS core/shell structure. Reproduced with permission.[53] Copyright 2020, ACS. **c)** Partial density of states (DOS) projected onto ZnS and $CsPbI_3$ of the four heterodimers. Purple and green curves indicate the contributions from $CsPbI_3$ and ZnS, respectively. The inset shows the schematic view of the band alignment for each interface structure. Reproduced with permission.[40] Copyright 2017, Wiley-VCH.

In type I core/shell structures, the shell material with wider bandgap can confine the carriers within the core. Besides, the shell material can also passivate the surface defects of the core material, resulting in an increase of their PLQY. Hence these structures are considered as suitable luminescent phosphors for applications in lighting, displays, ink-jet printing, etc.[54-56] The strategy of using one of the perovskite derivatives with larger bandgap, such as Cs_4PbX_6, as the shell material was proposed and demonstrated by Kaur *et al*.[52] (**Figure 2**a). In such structures, the protective Cs_4PbBr_6 shell is used to prevent degradation of the perovskite core and to ensure ample large-band offsets, enabling the excitons to follow the

carrier dynamics as in the type I core/shell system. Moreover, Xu *et al*.[45] used solution-grown $CsPbBr_3$ NCs embedded in Cs_4PbX_6 as the recombination layer to construct a LED. Compared with core-only $CsPbBr_3$ NCs, this all-perovskite and all-inorganic embedded core/shell NC composite showed usually fast exciton luminescence lifetime (90-300 ps at 10 K), which can be attributed to the enhanced oscillator strengths.

The type II core/shell structures are considered favorable for applications requiring electron and hole separation, such as solar cells, photoelectric devices and catalysis.[57-59] Li *et al*.[49] synthesized type II $CsPbBr_3/TiO_2$ core/shell structures, in which the PLQY was lower than the core only $CsPbBr_3$ NCs due to spatial charge separation. The band structure of $CsPbBr_3/TiO_2$ has an offset of conduction band and valence band by ~ -0.5 eV and ~ -1.2 eV, respectively, thus the TiO_2 shell provides a pathway for effective transfer of the photogenerated electron from the conduction band of the perovskite core to the conduction band of shell,[49] while photogenerated holes are confined within the core. Kong *et al*.[50] have also demonstrated that following shell formation, the PL emission of the $CsPbBr_3$/zeolites core/shell structure with staggered bandgap alignment was decreased due to the inhibition of radiative recombination process. It has been proposed, that with increasing loading of the $CsPbBr_3$ NCs into zeolites the photo-generated electrons transfer can be improved, making these NCs beneficial for applications, such as photocatalytic carbon dioxide reduction. Ravi *et al*.[53] reported a $CsPbBr_3$/ZnS pseudo-type II core/shell structure by using conventional ZnS semiconductor as a shell material. The valence band maxima of ZnS and $CsPbBr_3$ have comparable energy, while the conduction band minimum of ZnS is significantly higher (by ~ -2.2 eV) than that of the $CsPbBr_3$ core (Figure 2b). Comparable PL lifetimes measured for $CsPbBr_3$/ZnS on TiO_2 and on glass substrates, and extended PL lifetime observed on spiro-OMeTAD were explained by the electron confinement within the shell and delocalization of holes. These properties could

offer benefits for perovskite applications in optically pumped LEDs, photodetector and photocatalysis.

Besides the regular core/shell structures, other heterostructures such as heterodimers have been reported. Chen *et al*.[40] achieved epitaxial growth of wide bandgap (3.5 eV) shell of zinc blend to form the $CsPbX_3$/ZnS heterodimer. Figure 2c shows the partial density of states (DOS) for the $CsPbI_3$/ZnS heterodimer. A S plane is in contact with CsI plane (Figure 2c I), Zn connects with CsI (Figure 2c II), S with PbI_2 (Figure 2c III) and Zn with PbI_2 plane (Figure 2c IV), respectively, which was attributed to strong chemical hybridization between core and shell materials. The type I bandgap alignment is formed at the interfaces of S plane with CsI plane and Zn with PbI_2 (type-I, Figure 2c I and IV), and hence the electronic properties of $CsPbI_3$ determine the edges of valence and conduction band of $CsPbX_3$/ZnS heterodimer. For the interfaces of Zn in contact with CsI and S with PbI_2, the edge of valence band is contributed from ZnS and the edge of conduction band mainly comes from $CsPbI_3$ (type-II, Figure 2c II and III). Thus, the bandgap edges of heterostructures depend on not only the individual properties of the core and shell materials, but also the contact configuration, hybridization and interaction induced gap states.[40]

2.3 Lattice mismatch

In the core/shell structures, the effect of lattice mismatch should be considered when selecting a shell material. Lattice mismatch refers to the difference of lattice parameters between the core and shell materials. To achieve successful epitaxial growth of shell, lattice mismatch between the core and shell should be smaller than 15%.[41, 60-62] With larger lattice mismatch, large defect density and lattice strain at the core/shell interface are likely detrimental to the optical properties of NCs, e.g., reducing the PLQY. Lattice strain could also lead to an increase of surface energy, hence preventing the heterogeneous nucleation and epitaxial growth

of shell, resulting in lower shell thickness.[28, 63-66] With the gradual increase of the shell thickness, the difference in surface energy between the facets of the core increases, and preferential growth along the facets with lower energy is observed.[67] Therefore, small lattice mismatch between the core and shell materials is desirable to enable shell growth with optimal thickness. Zhang *et al*. developed a protocol for the synthesis of high-quality $FAPbBr_3/CsPbBr_3$ core/shell NCs with lattice mismatch of 3.4%.[41] Also, Yu group used PbS as an alternative shell material, which has small lattice mismatch (< 5%) with respect to the $CsPbI_3$ core, to prepare $CsPbI_3$/PbS core/shell structures. A passivation layer of PbS not only enhanced the PL efficiency, reduced the Stokes shift, narrowed the PL bandwidth, and increased the stability of $CsPbI_3$ NCs, but also switched the $CsPbI_3$ NC films from n-type behavior to nearly ambi-polar.[61]

The magnitude of the lattice strain in core/shell structures could also offer interesting opportunities for fine-tuning of the NC properties. Smith *et al*.[68] reported the use of lattice strain to tailor the optical and electronic properties of perovskite core/shell NCs. It was demonstrated that the formation of lattice-mismatched core/shell structures could change the conduction and valence band energies of both the core and the shell, hence tuning the NC light emission across a wide range of the electromagnetic spectrum, from the visible and the near-infrared ranges.[68] In the work conducted by Chen *et al*.,[69] it was reported that the piezoelectric polarization charge at the core/shell interface was formed due to relatively large lattice mismatch between the core $MAPbBr_3$ and the shell $(OA)_2PbBr_4$, leading to an internal electric field. It was suggested that the photogenerated excitons can cause light-induced screening of internal field, and thus improve multiphoton absorption cross-sections (σ_n) in $MAPbBr_3/(OA)_2PbBr_4$ NCs.[69] Therefore, choosing appropriate shell materials is highly desired, considering that lattice mismatch plays a vital role in the shell growth and affects the core/shell NC properties. In addition, considering perovskite nanocrystals with a formula of

ABX_3 have soft and ionic crystal lattices with cation sites such A^+ and B^{2+}, it is feasible to incorporate a variety of metal ions as dopants into the crystal lattices. Thus, metal ion doping could be beneficial in minimizing the lattice mismatch between the core and shell of perovskite nanocrystals, which is worth investigating in the future.

2.4 Defect tolerance

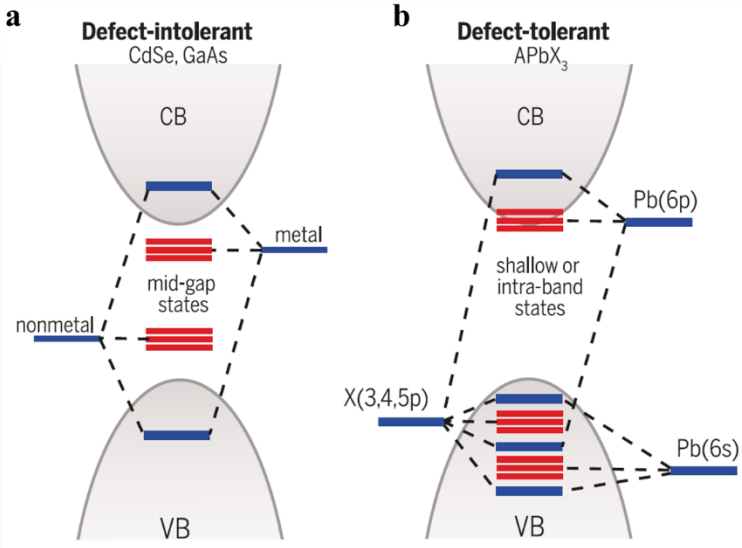

Figure 3 Schematic diagrams of electronic structures that are **a)** defect-intolerant (e.g. conventional semiconductors CdSe, GaAs, and InP) and **b)** defect tolerant (e.g. lead halide perovskites).[30] Copyright 2017, AAAS.

In conventional semiconductors, localized non-bonding or weakly bonding orbitals form trap states in the bandgap (**Figure 3**a). These inherent defects trap charges and act as scattering centers, which have a detrimental effect on the operational parameters of devices. Therefore, surface passivation is often required to improve the electronic and optical properties of NCs. In contrast, lead halide perovskite NC exhibit bright photoluminescence even without surface passivation due to their high defect tolerance. The low formation energy of vacancies in perovskite NCs results in a large number of Schottky-type (equal number of anion and cation

vacancies). A-site and halide vacancies, which can compensate each other since each vacancy type contributes an opposite charge carrier. Besides, the ions in the perovskite lattice have large bonding energy, and hence the interstitial and the antisite defects, which had been associated with the formation of deep defects, are virtually absent. Since the trap states formed by vacancies are observed either in the valence band or in the conduction bands, or as shallow defects; they do not significantly affect electronic and optical properties of perovskite NCs (Figure 3b). The perovskite is commonly described as a crystalline liquid due to the soft and dynamic properties of the lattice, and therefore the photo-induced carriers are less likely to be trapped and scattered.[70] At room temperature, polarons are formed by the electron and hole coupling, arising from the ionic character and strong structural dynamics of the PbX lattice, hence shielding the Coulomb potential and reducing the charge trapping and scattering between polarons and between polarons and charged defects or optical phonons.[30, 70]

Despite high defect tolerance, the defects existed in lead halide perovskite NCs still degrade their luminous properties. The PLQYs of perovskite NCs with fluorescence in the green-red range of the spectrum can only reach up to 80-90%. Besides, as an ionic structure, perovskite NCs are not very stable during purification and storage in harsh environmental conditions (e.g. exposure to air, polar solvent, heat and light). The interaction between surface ligands and atoms on the surface of perovskite nanocrystals is highly dynamic. During the purification process, the surface ligand shedding caused by polar solvents led to the increase of nanocrystalline defects, resulting in decomposition and loss of fluorescence properties. Hence, encapsulation perovskite NCs into a protective shell is one of the effective strategies to enhance their stability and accelerate the emergence of perovskite-based devices with enhanced performance.[41, 46, 70-72]

3. Synthesis and classification of core/shell structured perovskite nanocrystals

This section reviews the shell growth mechanisms in core/shell perovskite NCs, focusing on the following shell materials: perovskites and their derivatives, semiconductors, oxides, polymers, double- or multi-shell structures. Post-processing, epitaxial growth and ion exchange methods are utilized to overgrow a shell layer. Post-processing routes are considered, wherein the shell precursors are added into the solution containing pre-formed perovskite NCs. In the epitaxial growth methods, the shell precursors are introduced in the solution immediately after the formation of perovskite NC cores. Perovskites heterojunction modified with different halogens at the surfaces can also be obtained by an anion exchange method. **Table 1** summarizes the optical properties and applications of core/shell perovskite NCs reported to date.

Table 1 Summary of the optical properties and applications of core/shell perovskite NCs produced by various synthetic approaches.

Types of core/shell structure	Compound	Strategies	Shell synthesis strategy	PL Peak (nm)	FWHM (nm)	PLQY (%)	Application	Ref.
Perovskite shell	$CsPbBr_3/CsPbBr_{3-x}Cl_x$	Post-synthesis	Anion exchange	452, 520	/	/	/	[73]
Perovskite shell	$FAPbBr_3/CsPbBr_3$	*In-situ* synthesis	Heat-up	504	/	93	LED	[41]
Perovskite shell	$CsPbBr_3$/A-$CsPbBr_x$	*In-situ* synthesis	Hot-injection	463.4	32.87	84	LED	[74]
Perovskite derivative shell	$CsPbBr_3/Cs_4PbBr_6$	*In-situ* synthesis	Spin-coating	516	/	70	LED	[45]
Perovskite derivative shell	$CsPbBr_3/Cs_4PbBr_6$	*In-situ* synthesis	Hot-injection	516	/	96.2	/	[37]
Perovskite derivative shell	$CsPbBr_3/Rb_4PbBr_6$	Post-synthesis	Phase transformation and cation exchange	507	/	85	LED	[46]
Perovskite derivative shell	$MAPbBr_3/(OA_2MA_{n-1}Pb_nBr_{3n+1})$ (n = 1, 2, 3…)	*In-situ* synthesis	Ligand-assisted re-precipitation	519	/	92	/	[75]
Perovskite derivative shell	$MAPbBr_3/(OA)_2PbBr_4$	*In-situ* synthesis	Ligand-assisted re-precipitation	520	25	88	LED	[76]
Perovskite/semiconductor shell	$CsPbBr_3$/CdS	*In-situ* synthesis	Hot-injection	513	20	88	/	[77]
Perovskite/semiconductor shell	$CsPbBr_3$/nCdS/Al	*In-situ* synthesis	Hot-injection	512	<20	/	/	[78]
Perovskite/semiconductor shell	$CsPbI_3$/PbS	*In-situ* synthesis	Hot-injection	/	34	65	/	[61]
Perovskite/semiconductor shell	$CsPbBr_{3-x}I_x$/ZnS	*In-situ* synthesis	Wet chemical	/	/	73.6	/	[40]
Perovskite/oxide shell	$CsPbMnX_3/SiO_2$	Post-synthesis	Sol-gel	607	/	50.5	LED	[79]
Perovskite/oxide shell	$CsPbBr_3/SiO_2$	Post-synthesis	Hydrolysis and silanization	/	22	85	LED	[80]

Types of core/shell structure	Compound	Strategies	Synthesis methods	PL Peak (nm)	FWHM (nm)	PLQY (%)	Application	Ref.
Perovskite/oxide shell	$MAPbBr_3/ZrO_2$	Post-synthesis	Sol-gel	511	/	/	/	[81]
Perovskite/oxide shell	$CsPbBr_3/TiO_2$	Post-synthesis	Wet chemical and calcination	520	/	/	/	[49]
Perovskites/polymer shell	$CsPbBr_3$/poloxamer 127/PEG (15)-hydroxystearates	Post-synthesis	Emulsification-solvent evaporation	518	19	/	/	[82]
Perovskite/polymer shell	$CsPbBr_3$/PS-PEB-PS/PEG-PPG-PEG	Post-synthesis	Wet chemical	542	/	86	Bioimaging	[71]
Perovskite/polymer shell	$CsPbBr_3$/PMMA	Post-synthesis	Spray-assisted	515	20	73	Bioimaging	[42]
Perovskite/double- or multi-shell	$MAPbBr_3/SiO_2$/PVDF	Post-synthesis	Capillary forces	530	27	80	LED	[83]
Perovskite/double- or multi-shell	$CsPbBr_3/SiO_2/Al_2O_3$	Post-synthesis	Sol-gel	519	25	90	LED	[84]
Perovskite/double- or multi-shell	$CsPbBr_3$/MPMs/SiO_2	Post-synthesis	Hydrolysis-encapsulation	518	23	84	LED	[39]
Other type	$CsPbBr_3$/ZIF	*In-situ* synthesis	Wet chemical	/	/	/	Photocatalysis	[50]
Other type	$CsPbBr_3/Ta_2O_5$	Post-synthesis	Sol-gel	519	19	85	LED	[85]
Other type	$CsPbBr_3$/glass	*In-situ* synthesis	melt-growth processes	530	30	81.1	LED	[86]

3.1 Perovskites and their derivative shells

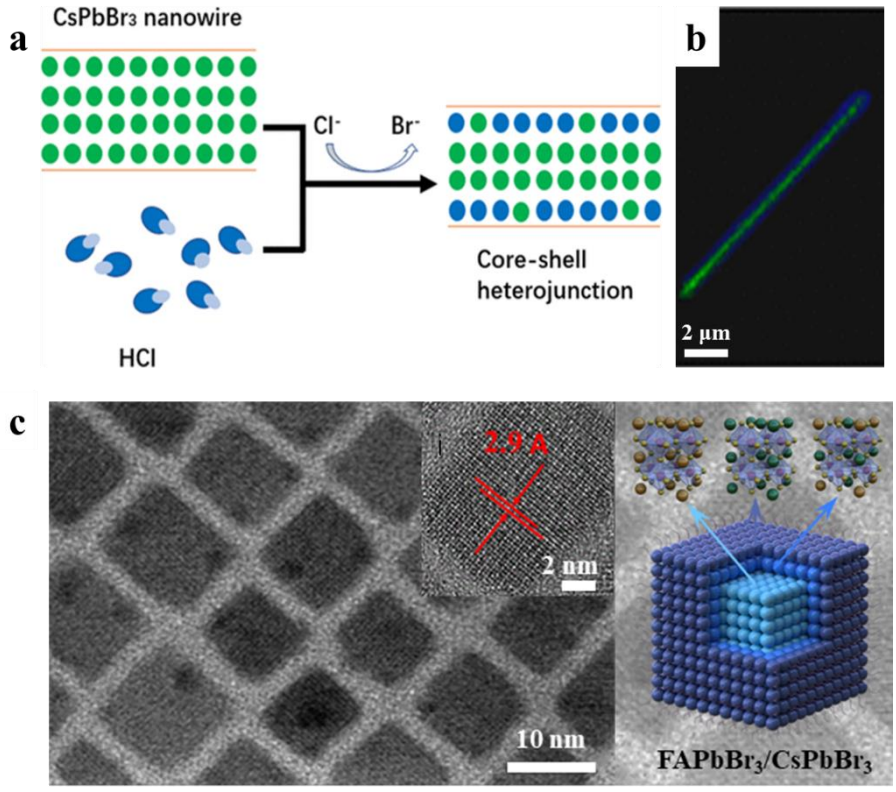

Figure 4 a) Schematic of $CsPbBr_3/CsPbBr_{3-x}Cl_x$ core/shell heterojunction formation mechanism and **b)** photograph (acquired at an excitation wavelength of 405 nm) of $CsPbBr_3/CsPbBr_{3-x}Cl_x$ core/shell heterojunction NWs. Reproduced with permission.[73] Copyright 2020, ACS. **c)** Transmission electron microscopic (TEM) and HRTEM (Inset) images and the structure of core/alloyed-shell/shell $FAPbBr_3/FA_xCs_{1-x}PbBr_3/CsPbBr_3$ perovskite NCs. Reproduced with permission.[41] Copyright 2020, Wiley-VCH.

3.1.1 Perovskite shell

As the halogen (X) site of perovskite NCs has highly ionic nature, the PL emission can be tuned by their composition, with halogen content being modified by an anion exchange reaction[87, 88] In this straightforward chemical reaction, foreign anions are introduced into a reaction mixture and replace the original anions in the parent NCs while retaining the NC morphology.[89] Zhang *et al.*[73] have employed an anion exchange approach to prepare $CsPbBr_3/CsPbBr_{3-x}Cl_x$ core/shell heterojunction nanowires (NWs). By introducing the source

of chlorine (HCl) in vapor phase rather than solution, the rate of the reaction was reduced to enabled facile control of the anion exchange process (**Figure 4**a). The exchange time, temperature and amount of added Cl^- play important roles in the formation of $CsPbBr_3/CsPbBr_{3-x}Cl_x$ core/shell heterojunction NWs. Using reaction conditions including a higher temperature (T > 30 °C), longer reaction time and higher Cl^- concentration, homogeneous alloyed $CsPbBr_{3-x}Cl_x$ NWs were produced. The synthesized $CsPbBr_3/CsPbBr_{3-x}Cl_x$ heterojunction NWs show two PL peaks at 520 nm and 452 nm, corresponding to the emission from the core and shell, respectively (Figure 4b). The anion exchange reaction provides a facile route to synthesize core/shell heterojunction perovskite NCs.

In-situ synthesis also provides a promising route to grow core/shell perovskite NCs. Recently, our group reported an epitaxial growth strategy to prepare stable $FAPbBr_3/CsPbBr_3$ core/shell NCs with a high PLQY of 93% (Figure 4c).[41] In this method, $FAPbBr_3$ NCs were synthesized through a hot injection method, where the crude solution of $FAPbBr_3$ NCs was directly used for $CsPbBr_3$ shell growth by adding Cs_2CO_3, $PbBr_2$, OA and oleylamine (OLA). The formation of an intermediate alloyed layer of $FA_xCs_{1-x}PbBr_3$ in these core/shell structures alleviates the lattice mismatch between the core and the shell. As the molar ratio of Cs: FA increases to 1: 1, the all-inorganic shell of $CsPbBr_3$ was formed on top of the transitional alloyed $FA_xCs_{1-x}PbBr_3$ layer. The produced $FAPbBr_3/CsPbBr_3$ core/shell NCs had an average size of 11.2 ± 1.1 nm and a PLQY of up to 93%.[41] A similar strategy has been employed by Xu *et al*.[90] who synthesized Mn-doped $CsPbCl_3$: $Mn^{2+}/CsPbCl_3$ core/shell NCs. In a typical synthesis, Mn^{2+}-doped $CsPbCl_3$ NCs were prepared by a ligand-assisted precipitation method. The oleylammonium chloride was added into the Mn^{2+}-doped $CsPbCl_3$ NC solution together with a precursor solution containing CsAc, $PbAc_2$, OA and OLA. The $CsPbCl_3$ shell was demonstrated to efficiently internalize the surface-bound dopant Mn^{2+} ions, resulting in an enhanced luminescence emission associated with Mn^{2+} impurities.[91-93] After the shell growth, the

average size of NCs have increased from 7 nm for core only and to 8.5 nm for the core/shell NCs. An increase in size was accompanied by an enhancement of PLQY (up to 39%). The epitaxial growth strategy is currently considered as the most promising strategy for the synthesis of core/shell perovskite NCs.

Wang *et al.*[74] synthesized cubic-shaped core/shell $CsPbBr_3$/amorphous $CsPbBr_x$ perovskite NCs using a hot injection method (T = 70 °C), followed by a centrifugation process to remove the byproduct of nanoplates. Compared to the $CsPbBr_3$ NCs near the heating center (bottom of the three-neck flask), the NCs in the supernatant are more likely to overgrow the amorphous shell due to the lack of enough energy for crystallization. The amorphous $CsPbBr_x$ shell prevents the surfaces of the $CsPbBr_3$ NCs from deterioration as evident from a high PLQY of up to 84% achieved in $CsPbBr_3$/amorphous $CsPbBr_x$ NCs, while its PL emission is stable under a high radiative intensity.[74, 94]

3.1.2 Perovskite derivative shell

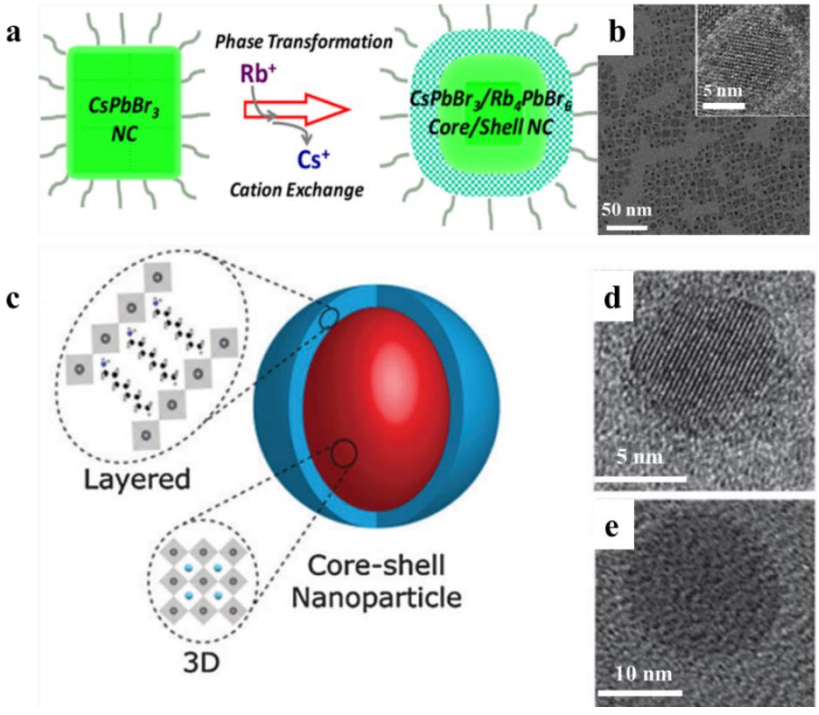

Figure 5 a) Schematic diagram of $CsPbBr_3/Rb_4PbBr_6$ core/shell NCs and **b)** TEM and HRTEM (insert) images of $CsPbBr_3/Rb_4PbBr_6$ NCs. Reproduced with permission.[46] Copyright 2018, ACS. **c)** Schematics diagram showing the core/shell type growth of a layer of octylammonium lead bromide nanomaterials over $MAPbBr_3$ NPs. **d)** and **e)** TEM images of core/shell NCs with MABr and OABr molar ratios 8: 2 and 3: 7, respectively. Reproduced with permission.[75] Copyright 2016, RSC.

Zero-dimensional (0D) perovskites with high exciton binding energy and wide bandgap have higher structural stability in the ambient atmosphere than 3D perovskite NCs.[37, 45, 95, 96] Jia *et al.*[37] used a seeded growth approach to synthesize core/shell $CsPbBr_3/Cs_4PbBr_6$ perovskite NCs. The Cs_4PbBr_6 shell was grown by successively adding zinc bromide and cesium oleate into the $CsPbBr_3$ seed solution at T = 70 °C. The shell thicknesses of thin-shell and thick-shell $CsPbBr_3/Cs_4PbBr_6$ of 1.6 nm and 3.1 nm were achieved by changing the amount of zinc bromide (0.1 mmol and 0.2 mmol), respectively. Since Cs_4PbBr_6 has a large bandgap of 4.0 eV, the Cs_4PbBr_6 shell can confine the photogenerated excitons in the $CsPbBr_3$ NC core. The formed $CsPbBr_3/Cs_4PbBr_6$ core/shell perovskite NCs have a PLQY of up to 96.2%, which is 12% higher than that of the core $CsPbBr_3$ NCs.[37] Wang *et al.*[46] developed a controlled post-synthesis phase transformation strategy to produce stable $CsPbBr_3/Rb_4PbBr_6$ core/shell NCs with a high PLQY of 85% (**Figure 5**a-b). It is proposed that the introduced rubidium oleate triggers the phase transformation while the Rb_4PbBr_6 shell is formed by the cation-exchange process.[97] The phase transformation and the cation-exchange occur on the surface of the $CsPbBr_3$ NCs, promoting the shell growth. Compared to perovskite NCs coated with Cs_4PbBr_6 shell, those capped with a Rb_4PbBr_6 shell have enhanced structural stability, due to the higher thermodynamic stability of Rb_4PbBr_6 shell.[46]

Encapsulation of a narrow bandgap 3D perovskite NCs with a wider bandgap 2D-layered perovskite shell could also enhance the stability of perovskite NCs. Bhaumik *et al.*[75] employed ligand assisted re-precipitation strategy to synthesize core/shell $MAPbBr_3/(OA_2MA_{n-}$

$_1Pb_nBr_{3n+1}$) (OA=$C_8H_{17}NH_3$, n = 1, 2, 3…) perovskite NCs (Figure 5c). The cation molar ratio, MA: OA, was used to control the size of core/shell NCs, and the NCs were formed with an average diameter from 5 to 12 nm with the molar ratio increasing from 8: 2 to 3: 7 (Figure 5d-e). The highest PLQY of up to 92% was achieved in mixed cation MABr-OABr NCs produced with MA: OA = 8: 2. A similar strategy has been employed by Vijila *et al*.,[76] who reported the synthesis of core/shell $MAPbBr_3/(OA)_2PbBr_4$ NCs, in which the $(OA)_2PbBr_4$ shell was formed by adding MABr and OABr with controlled molar ratios into the reaction solution during synthesis. The Stokes shift increased from 990 to 1138 meV when the MABr to OABr ratio was changed from 10:0 to 6:4 due to the reduction of the $MAPbBr_3$ core size and the over coating of a number of shell layers of $(OA)_2PbBr_4$ with a larger bandgap than the $MAPbBr_3$ core. The PL intensity of the synthesized core/shell NCs was increased due to improved confined excitonic recombination,[75] manifested by a large Stokes shift. A large Stokes shift is beneficial for enhancing PL stability and PLQY due to the negligibly small re-absorption of emitted light.[98] The synthesized $MAPbBr_3/(OA)_2PbBr_4$ NCs with a core diameter of 1-2 nm and a shell thickness of 4 nm also revealed the multiphoton absorption characteristics. The simultaneous absorption of multiple infrared photons leads to an excitation of electrons to a higher energy state and subsequent relaxation with shorter emission wavelengths, which is of interest for applications in multiphoton imaging applications.[69]

3.2 Semiconductor shell

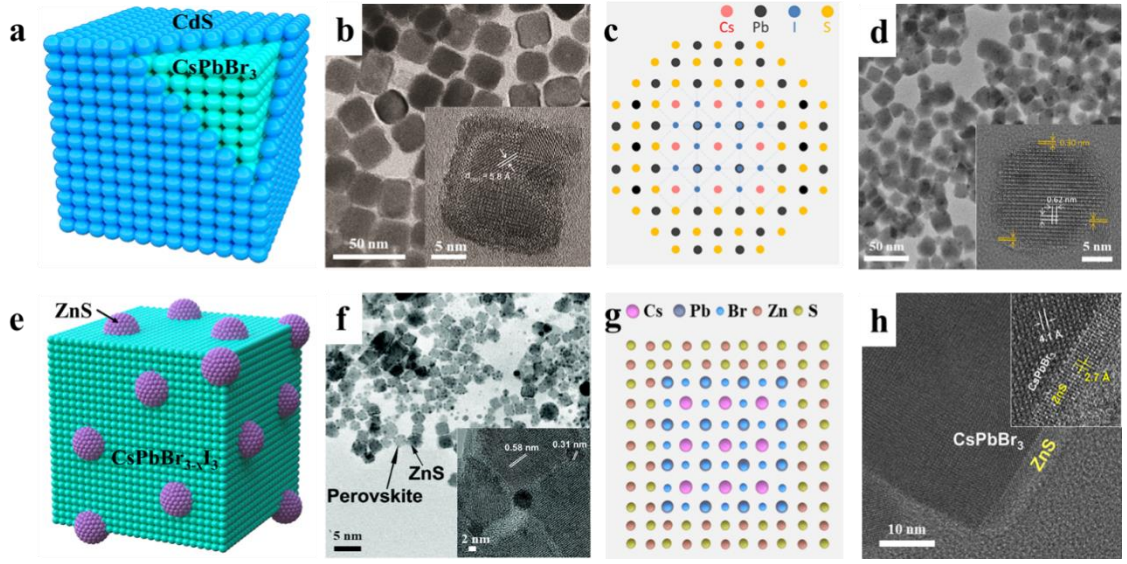

Figure 6 a) Schematic illustrations of core/shell $CsPbBr_3$/CdS NCs. **b)** TEM and HRTEM (Inset) image of $CsPbBr_3$/CdS NCs. Reproduced with permission.[77] Copyright 2019, Wiley-VCH. **c)** Proposed architecture of PbS capped $CsPbI_3$ NCs, and **d)** TEM images of $CsPbI_3$ NCs, the inset shows the HRTEM image of PbS capped $CsPbI_3$ NCs. Reproduced with permission.[61] Copyright 2018, ACS. **e)** Proposed architecture made of $CsPbBr_{3-x}I_x$/ZnS heterostructures. **f)** TEM images of $CsPbBr_{3-x}I_x$/ZnS heterodimers. Inset shows the HRTEM image of $CsPbBr_{3-x}I_x$/ZnS heterodimers. Reproduced with permission.[40] Copyright 2017, Wiley-VCH. **g)** Proposed architecture of $CsPbBr_3$/ZnS NCs. **h)** TEM and HRTEM (Inset) image of $CsPbBr_3$/ZnS core/shell NCs. Reproduced with permission.[53] Copyright 2020, ACS.

Apart from perovskites and their derivatives, binary II-VI and IV-VI semiconductors have been used as the shell material to improve the stability and optoelectronic properties of perovskite NCs.[26, 27, 47, 61, 77, 96, 99, 100] The efficiency of these materials in surface defect passivation has been originally developed for and demonstrated in the core/shell semiconductor NCs, such as CdSe/ZnS[101] and CdTe/ZnS.[102] Tang *et al*.[47, 77] reported a continuous injection method to prepare $CsPbBr_3$/CdS NCs. The Cd-oleate and OLA-S were selected as the shell precursors to grow a thin CdS shell. The formed $CsPbBr_3$/CdS core/shell NCs had an average size of 21.3 nm and a shell thickness of 2.5 nm (**Figure 6**a-b). After shell growth, the PL and absorption spectra of the $CsPbBr_3$/CdS NCs were blue-shifted compared with those of core only

$CsPbBr_3$ NCs. This blue shift indicates an increase of the bandgap of $CsPbBr_3$/CdS NCs, which was attributed to the Cd^{2+} ion diffusion into the NC core and the partial replacement of Pb ions by Cd^{2+} ions.[103, 104] An improved stability and enhanced PLQY (88%) were achieved in these core-shell NCs compared with the core only NCs. The reduced nonradiative recombination ratio (97% for $CsPbBr_3$ NCs and 91% for $CsPbBr_3$/CdS NCs) indicated that the synthesized $CsPbBr_3$/CdS NCs had lower Auger recombination and reduced fluorescence intermittency.[77]

Liu *et al*.[78] used the same CdS precursor to prepare $CsPbBr_3$/mCdS NCs (m is the number of precursor injections) by adding the precursors at different reaction times. Continuous blue shift of the PL and the absorption spectra of $CsPbBr_3$/CdS NCs and decrease of the PL intensity was observed during the CdS shell growth.[105] To further improve the optical stability of these NCs, a precursor solution containing aluminum isopropoxide was introduced into the reaction solution to initiate the growth of the aluminum hydroxide shell over $CsPbBr_3$/CdS NCs. The formation of a dense protective oxide layer was accelerated by exposure of $CsPbBr_3$/CdS/Al NCs to air. The resulting core/shell/shell structures exhibited long-term optical and structural stability.[105]

The core/sell strategy to enhance the optical properties and stability of perovskite NCs was also demonstrated for the other NCs with different halogens, such as $CsPbI_3$.[61] In this study, thioacetamide was used as S-precursor to control the size of PbS clusters. The shape of synthesized NCs changed from cubes to spheres with increasing S-content. The $CsPbI_3$/PbS NCs (Figure 6c-d) obtained using the molar ratio of S: Pb = 0.1 had PLQY of 65% and a narrow optical line-width (FWHM = 34 nm). In the $CsPbI_3$ films, the adjacent NCs shared one PbS cluster, which was shown to be beneficial for improved charge transport within the film, therefore resulting in a better LED performance.[106] The $CsPbBr_{3-x}I_x$/ZnS heterodimers were synthesized by Chen *et al*.[40] using a facile solution-phase method with zinc stearate and 1-dodecanethiol as zinc and sulfur precursors, respectively (Figure 6e-f). The observed PL peak

shift for the $CsPbBr_{3-x}I_x$/ZnS NCs was attributed to the presence of a wide bandgap ZnS shell. Moreover, increasing sulfurization time was shown to improve the PL lifetime and to increase charge diffusion length in light-absorbing materials, offering benefits for the NC applications in photovoltaic devices.

To date, both type-I and type-II heterojunctions were realized for the $CsPbBr_{3-x}I_x$/ZnS NCs.[40] Ravi *et al.*[53] used a zinc diethyldithiocarbamate ($Zn(DDTC)_2$),[107] as a single molecular precursor to prepare $CsPbBr_3$/ZnS core/shell NCs. The slow release of both Zn and S monomer species from the single source precursor at an elevated temperature (T = 120 ^oC) prevented self-nucleation of ZnS NCs and thus facilitated shell growth, forming stable $CsPbBr_3$/ZnS core/shell NCs (Figure 6g). The duration of thermal treatment needs to be carefully controlled, and as prolonged heat treatment (T > 100 °C), the $CsPbBr_3$ NCs were transformed into Cs_4PbBr_6, due to the loss of oleylammonium along with Br^- ions from the surface of $CsPbBr_3$ NCs. Hence, the excess amount of oleylammonium bromide was introduced into the reaction solution to retain the composition, structure and optical properties of NC core. The formed $CsPbBr_3$/ZnS NCs had an average size of 48.7 ± 7.9 nm (Figure 6h) and a 15-fold increase of the PL lifetime of $CsPbBr_3$/ZnS films up to 102.3 ns, compared to the $CsPbBr_3$ NC films.[53] The $CsPbBr_3$/ZnS NCs with improved PL lifetime are promising for applications in LEDs, photodetectors, and photocatalysis.

3.3 Perovskite/oxide shell

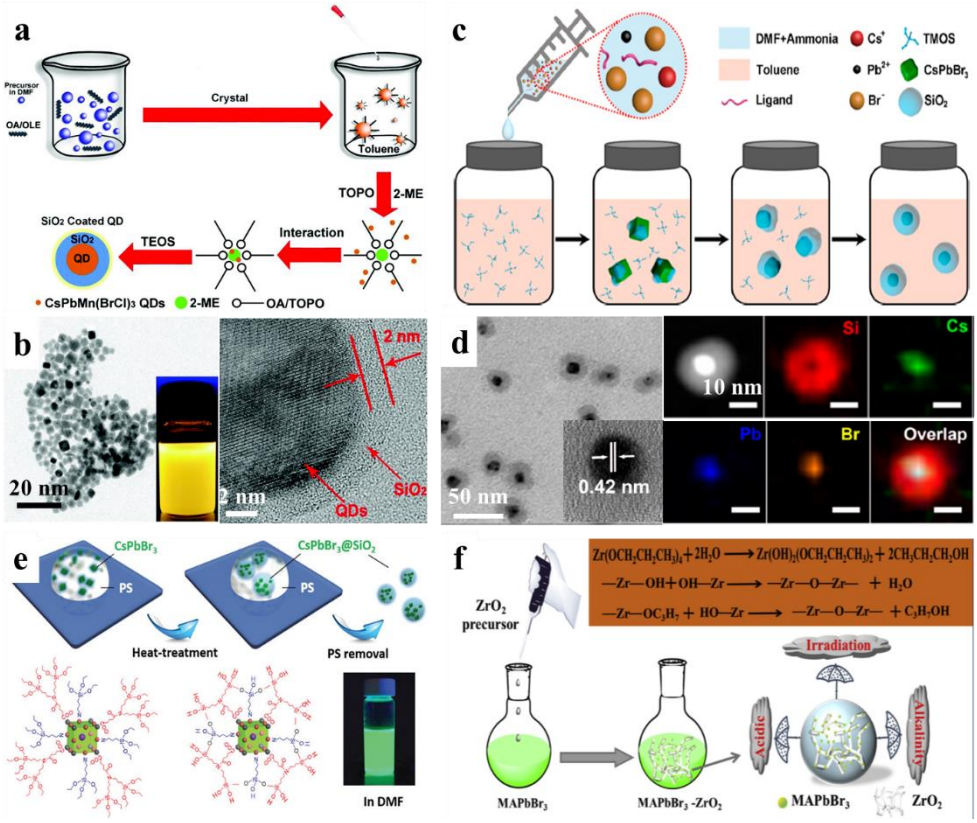

Figure 7 a) Schematic illustration of the procedure for synthesizing $CsPbMnX_3/SiO_2$ core/shell NCs. **b)** TEM and HRTEM images of $CsPbMnX_3$ NCs individually encapsulated within SiO_2 shells. Reproduced with permission.[79] Copyright 2019, Wiley-VCH. **c)** Proposed formation process of $CsPbBr_3/SiO_2$ core/shell NPs. **d)** TEM image of synthesized $CsPbBr_3/SiO_2$ core/shell NCs. Inset shows an HRTEM image of a single $CsPbBr_3/SiO_2$ NP, and HAADF-STEM image and elemental mapping images showing the elemental distribution of Si, Cs and Pb. Reproduced with permission.[108] Copyright 2018, ACS. **e)** Schematic illustration of the fabrication of high-stability $CsPbBr_3/SiO_2$ nanocomposites via confined condensation. Reproduced with permission.[109] Copyright 2018, RSC. **f)** Schematic illustrations of the formation process and enhanced acid, base and UV light resistance of $MAPbBr_3/ZrO_2$ nanocomposites. Reproduced with permission.[81] Copyright 2019, Elsevier BV.

Oxides such as silica (SiO_2)[38, 75, 79, 108-116], titanium oxide (TiO_2)[49, 117], alumina (Al_2O_3),[118] and zirconium oxide (ZrO_2)[51, 81] have been successfully used as the shell materials for the core-shell structured perovskite NCs to improve their mechanical rigidity and chemical stability. Although SiO_2 has been shown to improve photostability of semiconductor NCs, this

is not achieved in perovskites due to their strong ionic nature. The SiO_2 growth on perovskite NCs can be achieved by a direct hydrolysis method using tetraethyl orthosilicate (TEOS) as precursor.[79, 114] However, the presence of H_2O is detrimental to the properties of perovskite NCs. Tang *et al*.[79] introduced a multibranched TOPO capping ligand to reduce the interaction between the $CsPbMnX_3$ NCs and the water molecules, while 2-methoxyethanol (2-ME) was used as a catalyst to promote Si-O-Si matrix growth over the NC surfaces (**Figure 7**a-b). The successful growth of a SiO_2 shell on $CsPbMnX_3$ NCs was achieved with TEOS as the silica precursor through hydrolysis reactions:

$$Si\ (OR)_3 + 3H_2O = Si(OH)_3 + 3R - OH$$

$$Si - OH + HO - Si = Si - O - Si + H_2O$$

The amount of TEOS added was shown to directly affect the PLQY of NCs. The $CsPbMnX_3/SiO_2$ NCs synthesized with 200 μL TEOS (0.902 mmol) had a shell thickness of 2 nm and PLQY of 50.5%.[79] A similar strategy has been employed by Wang *et al*.,[114] who synthesized $CsPbBr_3$: Sn/SiO_2 by injecting the $CsPbBr_3$: Sn NCs into a toluene solution containing TMOS and ammonia. The amine groups in OLA surfactant and ammonia facilitate the hydrolysis of TMOS and absorb the hydrolysis products to form a silica shell. The amount of ammonia added was found to affect the NC properties and influence the thickness of shell by changing the hydrolysis rate.[114] Zhong *et al*.[108] reported a facile one-pot approach to synthesize $CsPbBr_3/SiO_2$ nanoparticles by injecting a mixture of perovskite precursors of CsBr and $PbBr_2$, the surfactant of OA and OLA, dimethylformamide (DMF) and ammonia solution into toluene containing TMOS (Figure 7c-d). The reaction time, temperature and ammonia content are optimized to control the size of the $CsPbBr_3/SiO_2$ nanoparticles. NCs with smaller size were produced in longer reaction time because of the dissolution of $CsPbBr_3$ NCs induced by ammonia.[108]

To develop a waterless reaction, Sun *et al.*[80] used (3-aminopropyl)triethoxysilane (APTES) as silica precursor and successfully synthesized $CsPbBr_3/SiO_2$ perovskite NCs by exposing the reaction mixture to the environment to capture the water vapor for the hydrolysis of APTES:

$$- SiOC_2H_5 - + H_2O \rightarrow - SiOH + C_2H_5OH$$

$$- SiOH + SiOC_2H_5 \rightarrow - SiOSi - + C_2H_5OH$$

$$- SiOH + - SiOH \rightarrow - SiOSi - + H_2O$$

The APTES amino groups coordinate to the surfaces of the perovskite NCs while three silyl ether groups are hydrolysed to form a cross-linked SiO_2 matrix. The core/shell $CsPbBr_3/SiO_2$ NCs have narrow FWHM (22 nm) and retain high PLQY (85%). In order to make perovskite NCs soluble in polar solvents, Cai *et al.*[109] synthesized $CsPbBr_3$ NCs using a ligand-assisted reprecipitation method in the presence of modified organosilicon ligand bis[3-(triethoxysilyl)propyl] amine with glutaric anhydride (BTPA-GA) and APTES. The synthesized $CsPbBr_3$ NCs were dispersed into polystyrene (PS) matrix, followed by a heat treatment to promote Si-O-Si cross-linking of surface ligands (Figure 7e). The PS matrix prevents aggregation of $CsPbBr_3/SiO_2$ and facilitates the formation of spherical $CsPbBr_3/SiO_2$ nanocomposites. The amino group from APTES enables the size control of perovskite NCs while the carboxyl group of BTPA-GA suppresses $CsPbBr_3$ NCs aggregation and improves their stability due to the coordination effect between the carboxyl group and surface Pb-ions.[119] Hydrobromic acid was used to ionize the amino groups to enhance electrostatic interactions with the surfaces of $CsPbBr_3$ NCs.

Liu *et al.*[51] utilized a modified interfacial approach to synthesize Janus $CsPbX_3/ZrO_2$ heterostructure NCs. Monodispersed Cs_4PbBr_6 NCs and $Zr(OC_4H_9)_4$ were blended in hexane, and then water was rapidly injected into the mixture and the $CsPbX_3/ZrO_2$ NCs were formed after ~ 12 h. In this method, Cs_4PbBr_6 transformed into $CsPbX_3$ NCs at the hexane/water

interface due to the dissolution of CsBr in water.[85, 120-122] However, it was shown that an amount of Zr precursor exceeding 10 μmol can generate undesirable hydrolytic byproducts, which deteriorates the structure of $CsPbBr_3$ and leads to the formation of ZrO_2 and $CsPbX_3$ NCs with large size distribution and uncontrolled shapes. The tunability of optical properties in the visible range of the spectrum was demonstrated for $CsPbX_3/ZrO_2$ with different halides, X = Cl/Br, Br, Br/I. This shell type was also successfully used to cap organic-inorganic perovskites. The $MAPbBr_3/ZrO_2$ nanoparticles were formed by[81] injecting zirconium n-propoxide, toluene and acetic acid into solution containing preformed $MAPbBr_3$ NCs. The traces of water in toluene and ambient environment were shown to assist the slow hydrolysis of zirconium n-propoxide and the formation of stable ZrO_2 sol with three-dimensional network structure (Figure 7f). A red-shift of PL peak from 503 nm to 511 nm was observed due to the change of NC size.[123, 124]

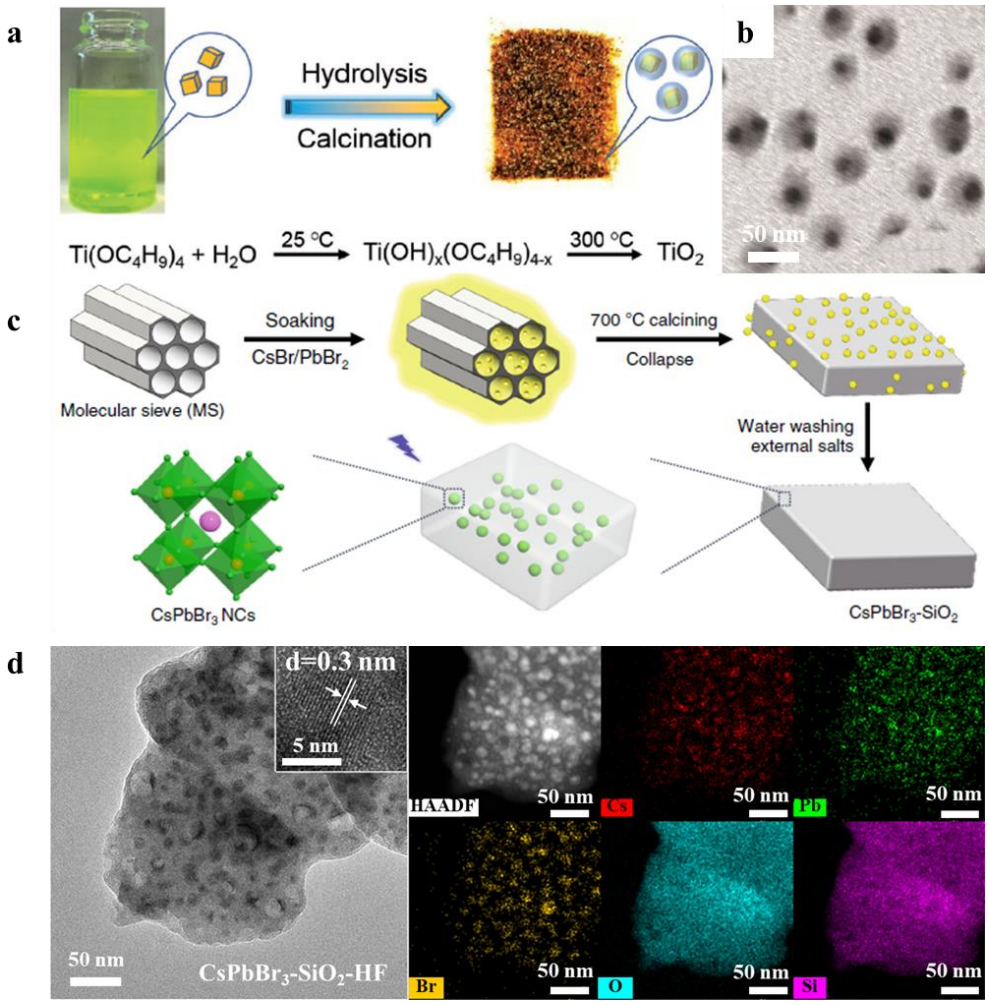

Figure 8 a) Schematic illustration of the fabrication process for the TiO_2-coated $CsPbBr_3/TiO_2$ core/shell NCs. **b)** $CsPbBr_3/TiO_2$ core/shell NCs after calcination at 300 °C for 5 h. Reproduced with permission.[49] Copyright 2017, Wiley-VCH. **c)** Schematic diagram of synthesis $CsPbBr_3$ NCs into SiO_2. **d)** TEM and HAADF-STEM images of $CsPbBr_3$-SiO_2-HF and the corresponding elemental mapping of Cs, Pb, Br, O, and Si. Reproduced with permission.[116] Copyright 2020, Springer Nature.

Except for the wet-chemical methods, the calcination process has also been used to produce core/shell perovskites. Li *et al.*[49] combined a wet-chemical method and a calcination process to prepare TiO_2-coated $CsPbBr_3$ NCs. Titanium butoxide (TBOT) was used as titanium precursor as it can hydrolyze at a low moisture level.[125] The TBOT precursor was added into $CsPbBr_3$ NCs dispersed toluene solution and the solution was stirred in 30% humidity at 25 °C to form $Ti(OH)_x(OC_4H_9)_{4-x}$.[126] A calcination process was conducted at T = 300 °C for 5 h to

remove water in order to obtain monodispersed $CsPbBr_3/TiO_2$ core/shell NCs with the TiO_2 shell thickness of 5 ± 3 nm (**Figure 8**a-b). The observed 'rounding' of the corners and edges of $CsPbBr_3/TiO_2$ NCs was attributed to the effect of water traces during the calcination process.[127]

Zhang *et al.*[116] synthesized stable and highly luminescent ceramic-like $CsPbBr_3$ NCs through *in-situ* encapsulation in a silicon molecular sieve (MS) template, which was selected as shell material due to its large surface area and small pore size (d = 3.6 nm).[128] The perovskite precursors such as CsBr and $PbBr_2$ permeated into the MS template and then it was dried at T = 80 °C, followed by a thermal treatment at T = 700 °C to strategically collapse the MS template hence forming SiO_2 protective layer (Figure 8c). The $CsPbBr_3/SiO_2$ structures exhibited the PLQY of 63%, which was further increased to 71% by HF etching process that removed un-encapsulated $CsPbBr_3$ NCs and decreased the shell thickness (Figure 8d).[116]

3.4 Perovskite/polymer shell

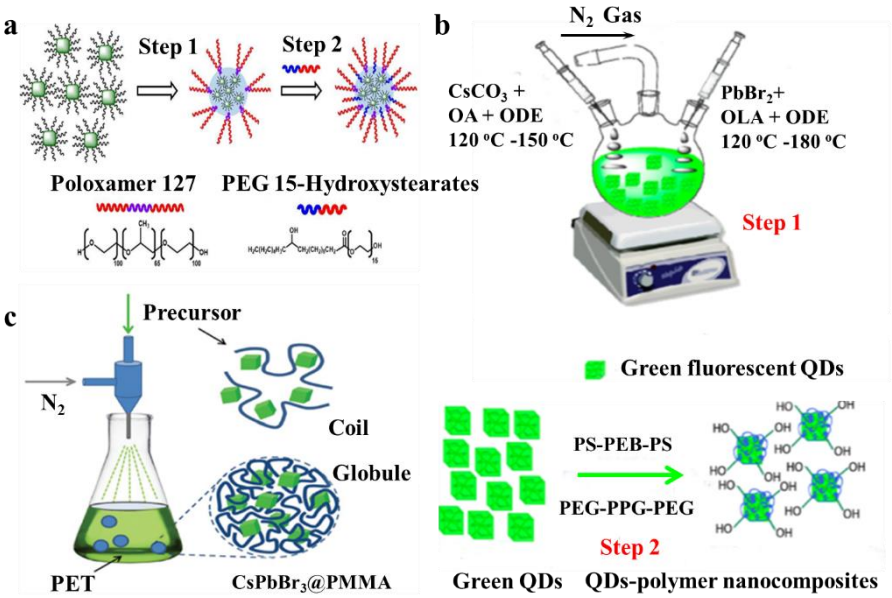

Figure 9 a) Schematic illustration of the encapsulation of hydrophobic $CsPbBr_3$ NCs in amphiphilic polymers to render them water-soluble. Reproduced with permission.[82] Copyright 2018, Wiley-VCH. **b)** Synthetic procedures used to develop (step 1) red fluorescence $CsPbBr_3$ NCs, (step 2) water-soluble PS-PEB-PS and PEG-PPG-PEG coated $CsPbBr_3$ NCs. Reproduced with permission.[71] Copyright 2019, ACS. **c)**

Schematic presentation of the spray-assisted precipitation method for preparing $CsPbBr_3$/PMMA nanospheres. Reproduced with permission.[42] Copyright 2018, Wiley-VCH.

In-situ encapsulation of perovskite NCs in a polymer shell provides another route to synthesize highly stable perovskite NCs.[42, 71, 129-132] Lee *et al*.[82] developed an emulsification-solvent evaporation strategy to coat $CsPbBr_3$ NCs with poly(ethyleneoxide)-poly(propyleneoxide)-poly(ethyleneoxide) triblock-copolymer (poloxamer 127) and polyethylene glycolylated hydrogenated castor oil (PEG (15)-hydroxystearates) (**Figure 9**a). In this synthesis, a phase transfer agent of poloxamer 127 was used to facilitate the nucleation of $CsPbBr_3$ during the emulsification process. Hydrophobic parts of the $CsPbBr_3$/poloxamer 127 nanocomposite interacted with long aliphatic hydrocarbon chain of PEG (15)-hydroxystearates to protect $CsPbBr_3$ core, while the water-soluble PEG moieties provide aqueous solubility of the nanocomposite. The formed $CsPbBr_3$/poloxamer 127/PEG-(15) hydroxystearate particles have a spherical shape with an average diameter of 55 nm and a narrow PL peak centered at 518 nm (FWHM = 19 nm). Moreover, the PEG shell provides protection against moisture and has low toxicity and reduced nonspecific biomolecule adsorption, making these perovskites potentially applicable for bioimaging.[133] A similar encapsulation strategy has been employed by Pramanik *et al*.,[71] who utilized polystyrene-block-poly(ethylene-ran-butylene)-block-polystyrene (PS-PEB-PS) and poly(ethylene glycol)-block-poly-(propylene glycol)-block-poly(ethylene glycol) (PEG-PPG-PEG) to synthesize $CsPbBr_3$/polymer composites (Figure 9b). Strong interaction was achieved between PS-PEB-PS and hydrophobic parts of $CsPbBr_3$ NCs, resulting in formation of stable $CsPbBr_3$/polymer composites with a high PLQY up to 88%. Moreover, the water-soluble PEG moiety acts as a protection layer to effectively prevent degradation of PQDs in water.[71]

Wang *et al*.[42] proposed a spray-assisted coil-globule transition method to synthesize $CsPbBr_3$-encapsulated PMMA nanospheres. In this approach, PVP was introduced as a

surfactant, and a mixture containing $CsPbBr_3$ NCs, dichloromethane and PMMA was sprayed onto nonpolar PET at a controlled liquid flow rate of 1 mL min^{-1} to form monodispersed $CsPbBr_3$/PMMA nanospheres (Figure 9c). In this method, intertwining interactions between PVP and PMMA polymer chains facilitate the coating of the PMMA onto the $CsPbBr_3$ NCs.[11] The molecular weight of PMMA did not affect the nanosphere morphology; however, its amount was shown to control the particle size: with increasing concentration of polymer larger spheres were formed. The synthesized water-soluble $CsPbBr_3$/PMMA nanospheres with an average size of 112 nm had a PL peak centered at 515 nm.[42] Other polymers, such as polystyrene (PS),[11, 131] hydrophobic semicrystalline polymer polyvinylidene fluoride (PVDF),[132] dielectric polymer matrix polyimide precursor dielectric (PIP),[129] semicrystalline and hydrophobic polyacrylonitrile (PAN)[130] and metal-organic-complex monomolecular intermediate ($[GaAA_3]_4$)[72] were also successfully used in core/shell structures to improve the stability and optical properties of perovskites for LEDs and solar cells, and bioimaging.[11, 72, 129, 132]

3.5 Perovskite/double- or multi-shell

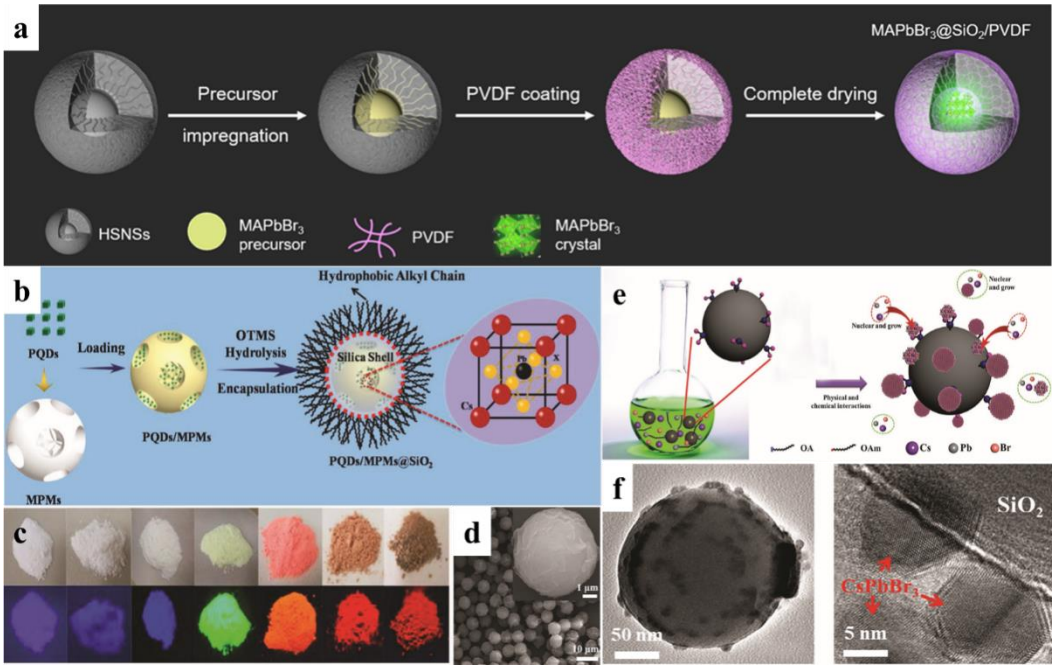

Figure 10 a) Schematic illustration of the synthesis procedures for the $MAPbBr_3/SiO_2$/PVDF NPs. Reproduced with permission.[83] Copyright 2019, ACS. **b)** Synthetic scheme of the $CsPbX_3$/MPMs/SiO_2 hybrid microspheres achieved via the hydrolysis-encapsulation strategy. **c)** Corresponding optical photographs of the $CsPbX_3$MPMs/SiO_2 hybrid microsphere powders with X changing from Cl to Br and I. **d)** $CsPbBr_3$/MPMs/SiO_2 hybrid microspheres. Insets are the corresponding enlarged SEM images of a single bare MPM and a single hybrid microsphere. Reproduced with permission.[39] Copyright 2019, Wiley-VCH. **e)** Schematic illustration of the synthetic strategy and fabrication of perovskite/SiO_2. **f)** TEM and HRTEM images of a typical $CsPbBr_3$ NCs/SiO_2 sphere. Reproduced with permission.[134] Copyright 2017, Wiley-VCH.

Although core/shell perovskite NCs can be synthesized using porous silica templates,[135, 136] their stability is limited by penetration of water and oxygen through the pores. To address this challenge, Huang *et al.*[83] developed a double-shell encapsulation strategy, where $MAPbBr_3$ precursor solutions were infiltrated into the hollow cavities of siliceous nanospheres via capillary forces, followed by PVDF coating to form $MAPbBr_3/SiO_2$/PVDF nanoparticles (**Figure 10**a). The concentration of $MAPbBr_3$ precursor was optimized to eliminate the growth of $MAPbBr_3$ outside the cavities, and the cavity size was used to control the NC size and hence their optical properties. With the cavity size increasing from 3.7 to 9.9 nm, the PL peak red-shifted from 525 to 533 nm with no change of FWHM. The $MAPbBr_3$ precursor concentration at 0.1 M was used to form $MAPbBr_3/SiO_2$/PVDF nanoparticles with an average cavity size of 6.1-8.2 nm and PLQY of 80%.

Li *et al.*[84] embedded $CsPbBr_3$ NCs into SiO_2/Al_2O_3 monolith through a sol-gel process blended with di-sec-butoxyaluminoxytriethoxysilane (DBATES) and $CsPbBr_3$ NCs dispersed in toluene. The single molecular precursor of DBATES contains two alkoxide functionalities and a typical Al-*O*-Si linkage, which facilitates formation of SiO_2/Al_2O_3 monolith in the absence of a catalyst.[137] Long branched DDAB was used as capping ligand for the synthesis

of $CsPbBr_3$ NCs in toluene with improved stability and PLQY, which was attributed to strong binding of Br^- ion of DDAB to the surface Pb^{2+} ions and to ligand steric hindrance to withstand exposure to water, alcohols or the sol-gel reaction.[138] The synthesized $CsPbBr_3/SiO_2/Al_2O_3$ monolith had a PLQY up to 90% and the PL peak red-shifted by 10 nm to 519 nm compared with $CsPbBr_3$ NCs core due to the increased reabsorption in $CsPbBr_3/SiO_2/Al_2O_3$ monolith.[84]

Recent reports indicated that the coating of 0D perovskite Cs_4PbBr_6 on 3D perovskite NCs could enhance the stability and optical properties of the latter.[37, 45, 95] Further enhancement of their stability was achieved by introducing an additional wrapping layer of silica matrix onto the surface of $CsPbBr_3/Cs_4PbBr_6$ NCs.[44, 139] In this approach, the surfactants such as OA and OLA were used to control the NC size and density of surface defects. The (3-aminopropyl) triethoxysilane (APTES) can attach to the $CsPbBr_3/Cs_4PbBr_6$ NCs and the silica matrix is formed by cross-linking reaction of $Si\text{-}O\text{-}C_2H_5$. The 0D Cs_4PbBr_6 also acts as a subshell for the NCs loaded onto mesoporous polystyrene microspheres (MPMs). The large surface areas and deep crosslinking channels of the MPMs provide protective loading platforms for perovskite applications in harsh solvents and/or high-temperature environments.[39, 140] The addition of SiO_2 shell not only seals the pores of MPMs to prevent perovskite leakage, but also further improves the solvent resistance by modifying the MPMs with ultralong alkyl chains (Figure 10b-d). The small red-shift of PL emission is observed for $CsPbBr_3/MPMs/SiO_2$ hybrid microspheres due to the change in the strength of quantum confinement induced by aggregation of $CsPbBr_3$ NCs in the microspheres. A small decrease of PLQY from 93% to 84% was ascribed to the multi-scattering effect and reabsorption caused by the MPMs microsphere and SiO_2 shell. Similar to other core/shell examples, tuning of the PL spectra can be realized in these structures from 395 to 690 nm by changing the halogen components (Figure 10c).[39]

3.6 Other types of shell

Combining perovskite NCs with zeolitic imidazolate framework (ZIF) can not only improve their moisture stability, but also adds new functionalities, such as enhanced capability in CO_2 capture due to the large specific surface area and highly active metal centers of ZIFs. Kong *et al*.[50] reported an *in-situ* synthetic process to directly grow ZIF on the surfaces of $CsPbBr_3$ NCs by dispersing $CsPbBr_3$ NCs in a precursor solution with metal ion and imidazole ligand. The size of the NCs increased from 5 to 9 nm due to the ripening of $CsPbBr_3$ NCs during a prolonged solution reaction process. With increasing concentration of zinc acetylacetonate/2-methylimidazole an increase of the particle size of $CsPbBr_3$/ZIF was obtained. These new structures combine complementary functionalities of the perovskite core and ZIF shell, hence offering exciting opportunities for their application in photocatalysis.[50]

Due to the good thermal, mechanical, and chemical stabilities, amorphous glasses have been employed as the host for various nanocrystals.[141-143] Inspired by the strategy widely used in traditional semiconductor NCs, such as CdSe[142], $CdS/Cd_{1-x}Zn_xS$ QDs[143], $CsPbX_3$ NCs-embedded glasses have been intensively investigated.[86, 144-149] Ye *et al.*[86] reported a melt-growth process to embed the $CsPbX_3$ into boro-germanate glasses. In this method, chemical powders, including PbO, Cs_2CO_3, NaX (X = Cl, Br, or I) and boro-germanate glasses were mixed thoroughly and melted at 1200 °C for 30 min, and then quenched to room temperature to form the as-prepared glasses. The Pb^{2+}, Cs^+, and I^- ions distributed homogeneously within the glass network, and these ions diffused and formed the $CsPbX_3$ NCs in the glass during further heat treatment. The PL of $CsPbX_3$ NCs embedded in the glasses can be tuned in a wide range by controlling the halide components and heat-treatment conditions ranging from 440 to 540 ^oC. Moreover, these $CsPbX_3$ NCs-embedded glasses exhibited good resistance to heating up to 200 °C and intense light irradiation up to > 2 W cm^{-2} due to the dense and inert nature of glass. Intense length irradiation-induced damage to $CsPbX_3$ NCs-embedded glasses can be recovered through thermal annealing. Other amorphous glasses, such as phosphate glasses[146],

tellurite glasses[150], borate glasses[149] and Zn-P-B-Sb based oxide glasses[151], have been also used to embed perovskite NCs and enhance the stability of perovskite NCs. These $CsPbX_3$ NCs-embedded glasses with good chemical, thermal, and photo stabilities, and high PLQY warrant the great potential for various applications, including LEDs, X-ray scintillation and random upconverted lasers.[86, 149-152]

Tunable PL of perovskite NCs with high PLQY is of particular interest for applications in lasing. Li *et al*.[134] reported a one-pot synthesis of perovskite NCs on the surfaces of monodispersed silica spheres (Figure 10e-f). Surface functionalization of the silica with amines was done to facilitate the formation of nucleation and growth points, and to enhance the interactions with $CsPbBr_3$ NCs,[3] resulting in a high PLQY to 56%. In this method, the change of anion composition allowed for tuning of the PL spectrum from 407 to 605 nm. This strategy has been applied for the synthesis of other perovskites, such as $FAPbBr_3$, $MAPbBr_3$ and Cs_2SnI_6.[134]

Hu *et al*.[85] synthesized a stable $CsPbX_3$/oxide Janus NCs by combining the water-triggered transformation process and sol-gel methods. The water-triggered process was used to transform Cs_4PbBr_6 NCs into $CsPbBr_3$ nanorods through CsBr extraction at the water-oil interface.[85, 120-122] Tetramethoxysilane (TMOS) has high hydrolysis rate and provides effective precursors for silica shell growth. The thickness of the silica on the Janus NCs was increased from 3.4 to 12.6 nm with increasing the amount of TMOS. The PL peak position of these Janus NCs can be tuned from 411 to 687 nm either by using different halogen Cs_4PbX_6 NCs or by the anion exchange process. This strategy was also applied for synthesis of other oxides Janus NCs, such as $CsPbBr_3/Ta_2O_5$ Janus NCs, which have a PL peak of 519 nm with an FWHM of 19 nm and a PLQY of 85%.[85]

4. Enhanced properties of core/shell perovskites

4.1 Enhanced optoelectronic properties

4.1.1 Optical properties

High PLQYs and long PL lifetimes are required for the applications in optoelectronic devices, such as LEDs. The PLQY is defined as the ratio of the radiative recombination rate to the total recombination rate:[153]

$$\eta = \frac{1/\tau_r}{1/\tau_r + 1/\tau_{nr}} \leq 1 \quad (1)$$

where τ_r and τ_{nr} are the radiative and non-radiative lifetime, respectively. $1/\tau_r$ and $1/\tau_{nr}$ represent corresponding recombination rates.

The PL decay time, the time before photoexcited carriers recombine, can be found from time-resolved PL studies, where the decay of PL intensity is fitted by a biexponential function:

$$A(t) = A_1 \exp\left(-\frac{t}{\tau_1}\right) + A_2 \exp\left(-\frac{t}{\tau_2}\right) \quad (2)$$

where A_1 and A_2 are constants, t is time, and τ_1 and τ_2 are decay lifetimes of nonradiative and radiative recombination, respectively.

In core/shell structures, the luminous properties of perovskite core, such as PLQY, PL lifetime, PL peak and FWHM, are modified by the effect of shell layer on the surface defect states and the electronic structure, as discussed above. Although the effects of the shell on the electronic properties of the perovskite cores depend on the core/shell interface types and the interactions at the core/shell interface, it is confirmed that the shell layer may eliminate the negative effect of the surface defect states, which act as traps for photo-generated carriers and provide non-radiative recombination sites, thus decreasing the PL emission.

To achieve the heterostructure-based core/shell perovskite NCs, the perovskite core is covered by a shell layer of a wider bandgap material,[37, 53, 95, 139] which affects by contact configuration, hybridization, and interaction induced gap states.[80, 154] For type I heterostructures, where both the electrons and holes are confined within the core, the shell

passivates surface traps hence enhancing the efficiency of radiative recombination process and helps to maintain a long-lived excited state for a slow PL decay process.[37, 40, 69] The quantum confinement of the photogenerated charge carriers induced by the shell also plays an important role in enhancing the luminous properties of perovskite cores.[51]

The beneficial role of the shell in passivation of surface defects and the exciton confinement was demonstrated for $FAPbBr_3/CsPbBr_3$ NCs synthesized with an intermediate layer of alloyed $FA_xCs_xPbBr_3$ by Zhang *et al.*[41] The core/shell NCs revealed significant improvement of the PLQY up to 93% (compared with 82% for core-only NCs) and an increase of the average PL lifetime (τ_{av}) from 30.2 to 40.1 ns. The exciton binding energy (E_b) for $FAPbBr_3/CsPbBr_3$ NCs was estimated to be 64 meV, corresponding to ~ 125% increase compared to $FAPbBr_3$ NCs (51 meV). Enhancement of the PLQY was also observed in other type I core/shell structures, such as $CsPbBr_3/Cs_4PbBr_6$,[37, 44, 45, 52, 139, 155] $CsPbBr_3/CsPbBr_{3-x}Cl_x$ nanowires,[73] $CsPbCl_3$: $Mn^{2+}/CsPbCl_3$,[90] $CsPbBr_3/Rb_4PbBr_6$,[46] $MAPbBr_3/(OA)_2PbBr_4$),[69] and $CH_3NH_3PbBr_3/NaNO_3$.[156]

The average lifetime for $CsPbBr_3$/ZnS core/shell NCs was increased to 102.6 ns, which is about 15 times longer than that of $CsPbBr_3$ NCs (7.2 ns).[53] This significant increase of PL lifetime was explained by the formation of pseudo type II band alignment at the core/shell interface, where the photoexcited electrons are confined inside the core while the holes are delocalized. In the case of $CsPbBr_3$/amorphous $CsPbBr_x$ core/shell NCs, the PLQY and τ_{av} were enhanced to 84% and 7.25 ns, respectively, compared to 54% and 6.68 ns for the core-only NCs. Moreover, the lifetime can be also modified by the power of the excitation source used, with amorphous layer facilitating enhanced light absorption by the core.[74] The prolonged carrier decay processes were also reported for other core/shell structures, such as $CsPbBr_3$/CdS NCs,[47] $CsPbMnX_3/SiO_2$ NCs,[79] $CsPbBr_3/SiO_2$ NCs[38, 80, 109, 112, 115] and $CsPbBr_3$/PbSe composite clusters[99], which exhibit nonblinking photoluminescence with high PLQY values.

Temperature-dependent optical studies of the $CsPbBr_3/SiO_2$ NCs also confirmed that exciton thermal dissociation leads to an increase of the PL lifetime from 50 to 410 ps with increasing temperature from 10 to 200 K. The monoexponentially decay of the PL observed in this structures further confirmed that the effective surface passivation decreased the number of luminescent trap states.[115] The enhanced PLQY and the prolonged lifetime, associated with beneficial effects of the shell, were reported for a number of structures, such as Janus nanoparticles (e.g. $CsPbX_3/SiO_2$, $CsPbBr_3/Ta_2O_5$ and $CsPbBr_3/ZrO_2$[51, 85]), for multi-shell capped NCs (e.g. $CsPbBr_3$/MPMs/SiO_2,[39] $CsPbBr_3/Cs_4PbBr_6/SiO_2$ NCs[44] and $MAPbBr_3/SiO_2$/PVDF[83]) and matrix-assisted quasi core/shell perovskites.[157] The size and spatial distribution of the perovskites in matrices can significantly affect their luminous properties.[157] For example, the $MAPbBr_3$/PVDF composite films exhibit enhanced PL properties with an optimized PLQY up to 94.6%, as a result of the separation of crystallization processes of PVDF and $MAPbBr_3$, which leads to uniform size and spatial distribution of NCs inside the matrix.[132]

4.1.2 Charge extraction ability

The charge carrier dynamic can be affected by the radiative and non-radiative recombination processes, as well as the charge extraction processes. Short charge separation distance and fast charge extraction are desirable for the perovskite NC application in solar cells. The photoexcited charge carriers would be quickly and efficiently collected at the core/shell interface, due to a short charge separation distance. It has been demonstrated that the interface containing the hole- or electron-extracting material can significantly reduce the charge separation distance, hence p- or n-type materials are intentionally used as the shell layer to enhance the charge carrier extraction efficiency.[158, 159] For example, monodispersed stable $CsPbBr_3/TiO_2$ core/shell NCs have been prepared by Zheng group,[49] in which type II

heterostructure band alignment led to the confinement of holes in the core and the delocalization of electrons. The fast charge transfer from $CsPbBr_3$ NCs to the TiO_2 shell was confirmed by observed decrease of the average lifetime (2.1 ns), compared to $CsPbBr_3$ NCs (14.8 ns). Furthermore, the $CH_3NH_3PbI_3$/copper thiocyanate (CuSCN) core/shell nanowires have been prepared on the TiO_2 film by Ashley *et al.*[157] These structures have radial and axial heterojunctions simultaneously, and the holes from perovskites are extracted by CuSCN at the radial heterojunction, while the electrons are extracted by TiO_2 at the axial junction, leading to a significant decrease of the average charge lifetime. Similar results were reported in the type II $CsPbI_3/ZrO_2$ NCs.[51]

4.2 Enhanced material stability

The key prerequisites for the advancement of the perovskite NCs into industry is their environmental stability and long shelf life. Encapsulation perovskite NCs into an inert protective shell is one of the common strategies to enhance their stability in different conditions, e.g. polar solvents, high temperatures and moisture.

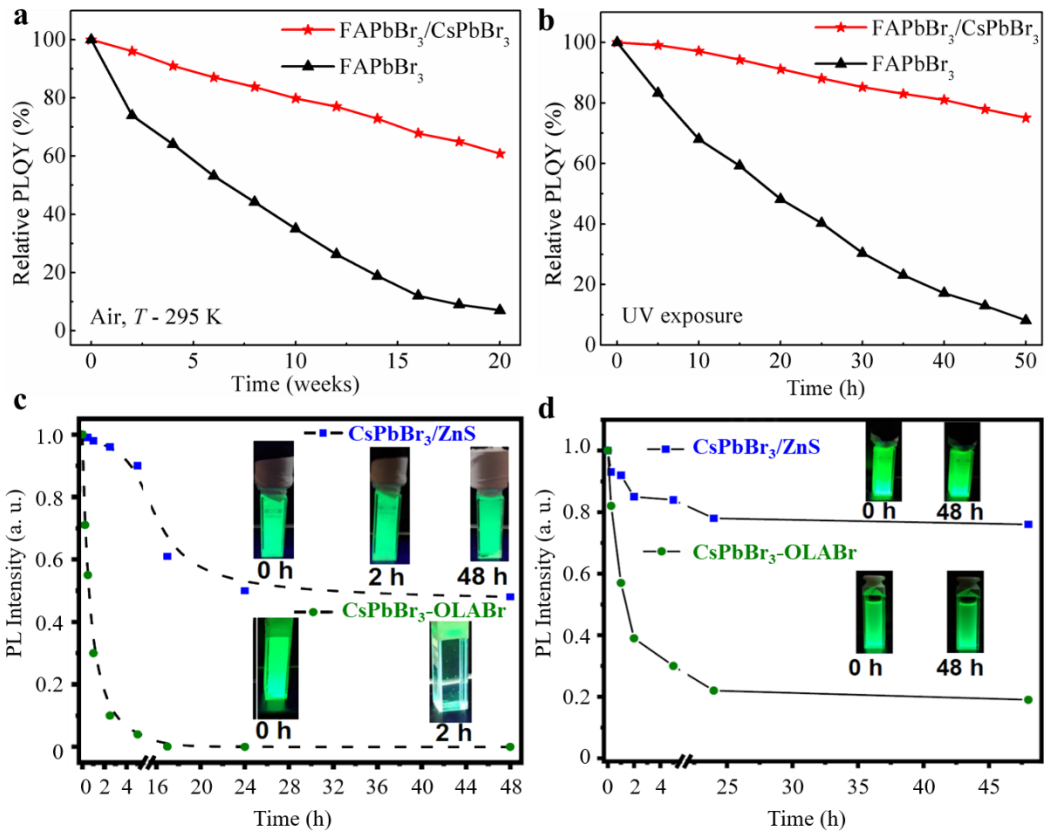

Figure 11 Time dependence of relative PLQY of $FAPbBr_3$ NCs and $FAPbBr_3/CsPbBr_3$ NCs **a)** under storage in ambient conditions and **b)** under exposure to 365 nm UV light. Reproduced with permission.[41] Copyright 2020, Wiley-VCH. **c)** Water stability tests on powder of $CsPbBr_3$/ZnS core/shell NCs and $CsPbBr_3$-OLABr NCs mixed with distilled water and PL spectra are recorded at regular intervals of time. **d)** PL intensity quenching of $CsPbBr_3$/ZnS core/shell NCs compared with that of $CsPbBr_3$-OLABr NCs irradiated with 50 mW white LED. Reproduced with permission.[53] Copyright 2020, ACS.

A number of studies focused on assessments of stability and shelf life of core/shell perovskite structures. Improved photostability was achieved for the epitaxially grown $FAPbBr_3/CsPbBr_3$ core/shell NCs, which retained their PLQY > 60% for over 20 weeks (**Figure 11**a) and ~ 80% of the initial PLQY after 50 h of UV illumination (Figure 11b).[41] A nearly constant PL intensity of $CsPbCl_3$: $Mn^{2+}/CsPbCl_3$ was observed after heating cycles from room temperature to 110 °C.[90] A small blue-shift during the heating cycle was attributed to

the lattice expansion, which resulted in an increase of Mn^{2+}-ligand distance and thus a smaller crystal field splitting.[93] Perovskite derivative shells, such as $CsPb_2Br_5$,[155] Cs_4PbBr_6,[37] $(Rb)_4PbBr_6$[46] and $(OA)_2PbBr_4$,[75] have also been explored to improve the NC properties. Despite significant improvement in the stability of NCs capped with perovskites and their derivatives, their long-term storage and stability under exposure to UV and elevated temperatures[75, 155] remains to be fully addressed.

Semiconductor compounds, such as ZnS, CdS and PbS, provide an effective shell to improve the stability of the perovskite NCs.[53, 61, 77] Ravi *et al*.[53] reported the ZnS shell coated $CsPbBr_3$ NCs by using $Zn(DDTC)_2$ as a precursor, which maintained 54% of their initial PL intensity after 48 h storage in solution with added distilled water, while the PL of the core-only NCs is quenched completely within 2 h at these conditions (Figure 11c). Enhanced photostability of the ZnS-capped NCs was also achieved, maintaining ~ 80% of initial PL intensity after 48 h of continuous irradiation with 50 mW white LED, compared with ~ 20% for core only NCs (Figure 11d). Tang *et al*.[77] utilized an epitaxial growth strategy to coat $CsPbBr_3$ NCs with CdS shell. The relative PL intensity of CdS encapsulated $CsPbBr_3$ NCs retained 83% of its original value during storage in 75% humidity for 14 h. Also, ~ 40% of initial PL intensity was retained after thermal treatment on these NCs at T = 60 °C for 9 h compared to full PL quenching for core only NCs.[77] In related work, $CsPbI_3$/PbS NCs[61] were integrated into LED devices, with only negligible changes of the electroluminescence intensity observed after 33 days of storage in ambient conditions, while the core-only LEDs maintained only 30-40% of the initial intensity. In the perovskite films with core-only NCs, the degradation of device performance is attributed to ion migration and generation of nonradiative recombination sites in the emissive layer.[160]

Enhanced stability was also reported for the perovskite NCs encapsulated into an inert protective polymer shell. $CsPbBr_3$/PMMA nanospheres reported by Wang *et al*.[42] retained 81%

and 92% of the original PL intensity after exposure to water and ethanol, respectively, for 80 days, and over 70% of their luminescence after 3 days exposure to UV irradiation; the fluorescence degradation under UV was attributed to the ageing of PMMA.[42] Yan *et al.*[43] prepared $CsPbBr_3$/mPEG-NH_2 NCs and reported an unexpected increase of the relative PL intensity from 100% to 130% after one week of storage in water. The enhanced PL intensity was ascribed to the crosslinking of mPEG-NH_2 on the NC surface, which leads to passivation of the surface non-radiative recombination centers.[161] It was proposed that the hydrophobic interaction between ethidene and water molecules and the hydration of oxygen atoms coordinated water molecules around the mPEG-NH_2 chains could provide water-resistance.[162] Moreover, the PL intensity of $CsPbBr_3$/mPEG-NH_2 NCs retained ~ 80% of the initial PL intensity at temperatures up to 100 °C.[43]

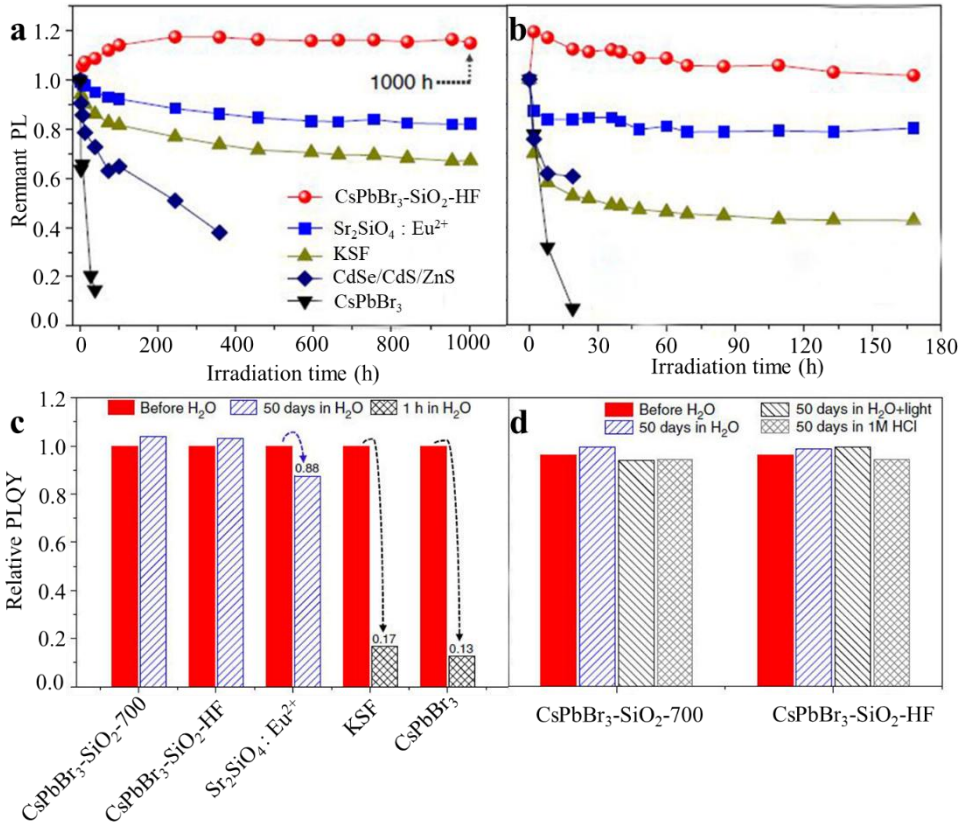

Figure 12 a) Photostability studies of different fluorescent materials under on the LED chips (20 mA, 2.7 V), and **b)** aged at T = 85 °C and 85% humidity conditions on the LED chips (20 mA, 2.7 V). **c)** Relative PLQYs of different fluorescent materials after immersed in water for various times. **d)** Relative PLQYs of

the $CsPbBr_3$-SiO_2-700 and $CsPbBr_3$-SiO_2-HF after immersed in various solvents for 50 days. Reproduced with permission.[116] Copyright 2020, Springer Nature.

Oxide shell coating of the perovskites has proved to be an effective way to suppress defects and enhance optical properties and to improve the chemical stability, photostability and water-resistance of the NCs. Song *et al*.[113] demonstrated that the $CsPbBr_3/SiO_2$ NCs can retain 41% of PL intensity in toluene/water solution (1:1 v/v), while PL quenching was observed for core only NCs. The decreased PL intensity of $CsPbBr_3/SiO_2$ was partially attributed to the decomposition of the core $CsPbBr_3$ NCs by alcohol molecules during the hydrolysis and polymerization of APTES and the effect of water.[113] Similarly, enhanced water tolerance was reported for $CsPbBr_3/SiO_2$[38, 79, 108, 110, 112, 115] and $CsPbBr_3$: Sn/SiO_2[114] compared with core only NCs. For the NCs with silica shell, the long soaking and stirring in water could lead to an increase of their size and gradual transformation to nanoplates, due to replacement of the surfactant (OA, OLA, TOPO, etc.) with the H_3O^+ and OH^- generated by water.[163, 164] More importantly, the PL emission of perovskite/SiO_2 NCs showed good recovery capability: the NCs retained ~ 96% of the initial PL intensity after temperature cycling from T = 30 to 160 ^oC,[110] and 72% of PL intensity following five repeats of the thermal cycle (T = 25 to 105 ^oC).[112] Highly luminescent $CsPbBr_3/SiO_2$-700 and $CsPbBr_3/SiO_2$-HF were synthesized by Zhang *et al*.[116] with improved water resistance and chemical stability compared to Sr_2SiO_4: Eu^{2+} and KSF red phosphors. These core/shell structures were formed using silicon molecular sieve template and had better operational stability compared with core-only $CsPbBr_3$ NCs, CdSe/CdS/ZnS NCs, ceramic Sr_2SiO_4: Eu^{2+} green phosphor, and even commercial KSF red phosphor, retaining ~ 100% of the original PLQY under illumination with blue LED for up to 1000 h and under thermal treatment (T = 85 °C) and humidity (85%) (**Figure 12**a-b). The $CsPbBr_3/SiO_2$-HF NCs also had retained the original value of PLQY after soaking in water or 1M HCl solution for 50 days (Figure 12c-d).[116]

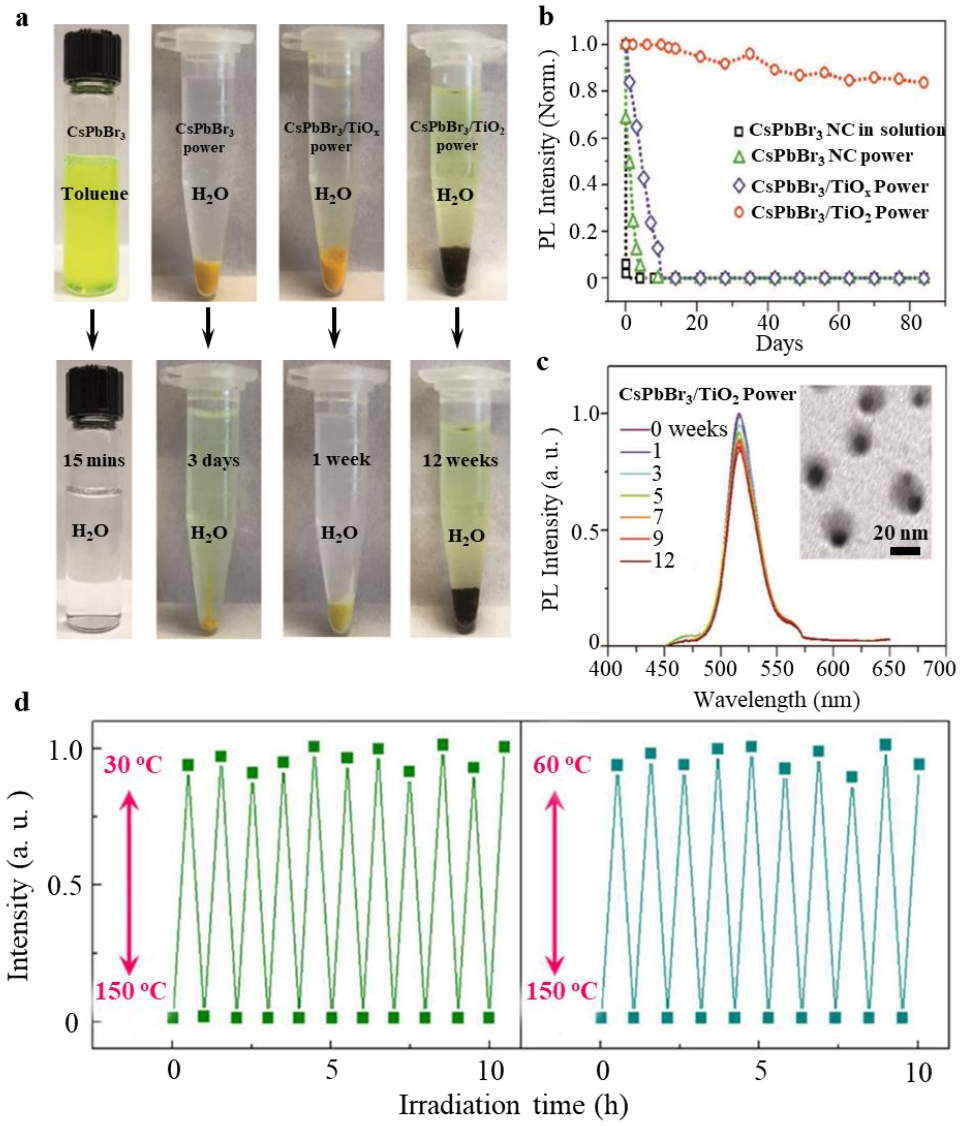

Figure 13 a) Optical images of the fresh $CsPbBr_3$ NCs in toluene, dried $CsPbBr_3$ NC powder in water, $CsPbBr_3/TiO_x$ composite in water, and $CsPbBr_3/TiO_2$ NCs in water (top) and different extended time under ambient conditions (bottom). **b)** Relative PL intensity of $CsPbBr_3$ NCs, dried $CsPbBr_3$ NC powder, $CsPbBr_3/TiO_x$ powder, and $CsPbBr_3/TiO_2$ NC powder after immersing in water; **c)** Relative PL intensity of $CsPbBr_3/TiO_2$ NCs after immersing in water (0-12 weeks), inset shows a TEM image of $CsPbBr_3/TiO_2$ NCs after immersing in water for 12 weeks. Reproduced with permission.[49] Copyright 2017, Wiley-VCH. **d)** $CsPbBr_3/Cs_4PbBr_6/SiO_2$ reversible fluorescent response of 10 consecutive cycles at 30-150 °C and 60-150 °C, respectively. Reproduced with permission.[44] Copyright 2017, ACS.

Similar to SiO_2, other oxides such as TiO_2 and ZrO_2 were also used as shell material to enhance the stability of perovskite NCs.[49, 51, 81] The $CsPbBr_3/TiO_2$ NCs maintained 85% of the initial PL intensity after 3 months storage, 75% under exposure to the UV light for up to 24 h, and their morphology was not affected by long term soaking in water (12 weeks) (**Figure 13**a-c).[49] Similarly, $CsPbBr_3/ZrO_2$ NCs maintained ~ 80% of initial PL intensity after 8 days in hexane/water solution.[51] Improvement of the NC stability is achieved by selections of the shell material, optimization of shell thickness and eliminations of pores in the shell layer.[108, 109, 113] To address these challenges, double-shell strategies were deployed.[44, 83] Significant enhancement of the NC stability was reported by Huang *et al*.[83] for double-shell $MAPbBr_3/SiO_2$/PVDF nanoparticles, which retained ~ 97% of the initial PL intensity after 2 months of storage in air with humidity of up to 94%. In photostability studies, these core/shell/shell structures retained 88% of initial intensity after 50 h UV exposure, which is higher compared to core $MAPbBr_3$, and single-shell $MAPbBr_3$/PVDF and $MAPbBr_3/SiO_2$.[83] Similar results were reported by Xu *et al*.[44] for $CsPbBr_3/Cs_4PbBr_6/SiO_2$/PDMS films, which demonstrated complete fluorescence recovery after ten heating-cooling cycles (T = 30 to 150 °C). These $CsPbBr_3/Cs_4PbBr_6/SiO_2$ samples have also shown excellent storage-stability with ~ 9% decrease of PL intensity after 2 months of storage in ambient conditions with 50% humidity (Figure 13d).[44]

5. Optoelectronic applications

Research into exploitation of perovskite materials in optoelectronics is rapidly expanding and is supported by advances in the synthesis of stable NCs, as well as investigations into fundamental properties of these materials, which underpin device performance. In this section, we highlight the applications of core/shell perovskite NCs in lighting and displays, solar cell, photodetector, and other promising applications.

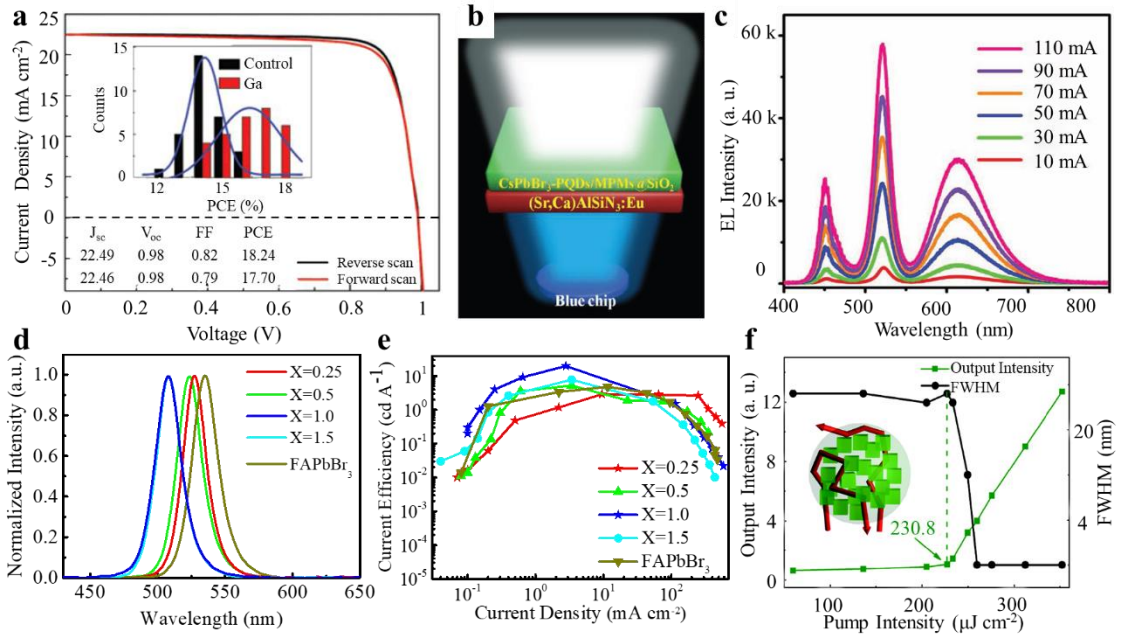

Figure 14 a) *J-V* curve of the perovskite solar cell with forward and reverse scan, inset shows the efficiency distribution with the control and Ga-1.5 solar cells. Reproduced with permission.[72] Copyright 2018, RSC. **b)** Schematic diagram of the fabricated phosphor-type white LED structure. **c)** EL spectra recorded at varying injection currents from 10 to110 mA. Reproduced with permission.[39] Copyright 2019, Wiley-VCH. **d)** EL spectra at an applied voltage of 5.5 V. **e)** Current efficiency-current density curves of the PeLEDs based on different molar ratio of Cs/FA. Reproduced with permission.[41] Copyright 2020, Wiley-VCH. **f)** ASE spectra for $CsPbBr_3/SiO_2$ films under femtosecond laser excitation at 800 nm, inset shows the schematic diagram for multiple light scattering with gain in $CsPbBr_3$ NCs embedded into a SiO_2 sphere. Reproduced with permission.[38] Copyright 2017, Wiley-VCH.

5.1 Solar cells

Perovskites have emerged as a promising class of light-harvesting materials suitable for applications in solar cells owing to their unique optoelectronic properties including high absorption coefficients, tunable direct bandgap and long charge carrier diffusion length. Recently, a record high power conversion efficiency (PCE) of 25.5% was achieved in perovskite solar cell;[165] however, their stability has been identified as the main drawback for commercialization. Li *et al.*[72] fabricated $Cs_xFA_{1-x}PbI_3/[GaAA_3]_4$ core/shell perovskite NCs by

introducing gallium (III) acetylacetonate ($GaAA_3$) as the precursor for *in-situ* formation of monomolecular metal-organic-complex intermediate ($[GaAA_3]_4$). Solar cell based on these core/shell perovskites showed a short-circuit current density, J_{SC} = of 22.48 mA cm^{-2}, an open-circuit voltage, V_{OC} = of 0.98 V, a fill factor, FF = 0.82 and a peak PCE of 18.24% (**Figure 14**a). The *J-V* curve under forward scan is almost identical to the reverse scan with only a small decrease of FF from 0.82 to 0.79. In addition, an improvement of the average PCE from 14% to 17% is achieved upon introduction of the $GaAA_3$. The performance enhancement was attributed to the epitaxial growth of ultra-thin $[GaAA_3]_4$ shell, capable of efficient passivation of deep trap-states at the core/shell interface.[72] More importantly, the solar cells with these core-shell perovskites showed significantly improved stability. The decrease of the device PCE is <10% over 800 h operation under 50% humidity conditions, while the efficiency of core-only NC devices declined by > 30%.[72] Hence, the core/shell structures could provide an effective strategy towards highly efficient and stable perovskite solar cells.

5.2 Lighting and display

LEDs fabricated with a layer of perovskite NCs as emitter exhibit superior luminescence and wide color gamut, and have attracted considerable attention in solid-state lighting and display fields.[79, 80, 85] The perovskite/SiO_2 core/shell NCs have been widely studied for such applications, as SiO_2 can improve perovskite stability and PLQY, and provides an optically transparent, chemically inert and non-toxic shell[39, 79, 80, 83, 85, 110, 112, 114, 115, 139, 166] Sun *et al*.[80] fabricated white LEDs (WLEDs) using a NCs/SiO_2 layer containing green $CsPbBr_3$ and red $CsPb(Br/I)_3$ perovskites deposited on blue-LEDs. Optical studies of these devices confirmed that anion exchange between red and green-emitting NCs was prevented by the presence of SiO_2 shell, and the devices demonstrated power efficiency of 61.2 lm W^{-1}, stable emission intensity over 10 h operation, and Commission International de l'Eclairage (CIE) color

coordinate of (0.33, 0.33) corresponding to 120% of the National Television System Committee (NTSC) standard.

Since agglomeration of the NCs was observed after capping with a thick SiO_2 shell (~ 4.2 nm), significant efforts have been devoted to developing a procedure for the synthesis of NCs with a thin SiO_2 shell.[108]. Tang *et al*.[79] reported a facile reverse microemulsion method (a versatile sol-gel method at room temperature) to synthesize core/shell Mn^{2+} doped $CsPbX_3$ (X = Br, Cl) NCs with a relatively thin SiO_2 shell of ~ 2 nm. The WLED device fabricated with a mixture of $CsPbMnX_3/SiO_2$ and $CsPbBr_3$ NCs on a UV GaN LED demonstrated luminous efficiency of 68.4 lm W^{-1} at 10 mA and only small change of color rendering index (CRI) (from 91 to 87) as the applied current increased from 10 to 200 mA. Hu *et al*.[85] produced monodisperse $CsPbX_3/SiO_2$ nanoparticles for the WLEDs and achieved color coordinate of (0.3, 0.32), CRI of 63 and 138% of NTSC standard gamut. The presence of SiO_2 shell ensured stability of color coordinates during continuous device operation of at least 1 h.

Organic materials are also advantageous as protective shells for perovskites. Zhou *et al*.[132] used PVDF, a hydrophobic semicrystalline polymer, as a matrix for $MAPbBr_3$ NCs to produce $MAPbBr_3$/PVDF composite films with PLQYs up to ~ 95%. The mechanical and piezoelectric properties of PVDF offer exciting potential for applications in flexible wearable electronics. The $MAPbBr_3$/PVDF films were embedded into UV cured adhesive with incorporated $K_2SiF_6:Mn^{4+}$ with red emissions. These films were successfully used in a prototype device of phosphor-converted white LED with a luminous efficiency up to 109 lm W^{-1} and color gamut of 121% NTSC standard at 20 mA current. Yoon *et al*.[154] demonstrated that dual-silicon nitride and silicon oxide ligands of the polysilazane (PSZ) inorganic polymer coated on $CsPbBr_3$ NCs increase the PLQY to ~ 82% and improve thermal, photo, air and humidity stability of the NCs. The WLED fabricated using these NCs had a high luminous efficacy of 138.6 lm W^{-1} and a

color gamut of 128% and 111% without and with color filters, respectively, at a correlated color temperature of 6762 K.

Double shell structures also proved to be beneficial for LED applications. The $CsPbBr_3$/MPMs/SiO_2 core/shell structures with green fluorescence, synthesized by Yang *et al*.,[39] were combined with red commercial phosphors (Figure 14b) on top of a blue emitting chip to form WLEDs with power efficiency of ≈ 55 lm W^{-1}, a chromatic coordinate of (0.33, 0.33) and a correlated color temperature of 5616 K under injection current of 10 mA. As shown in Figure 14c, the EL intensity was gradually enhanced with increasing injection current and the EL spectra have not revealed any measurable change after continuous device operation over 5 h. By combining commercial $K_2SiF_6:Mn^{4+}$ as red phosphors and a MPM material as a thermally insulated shroud, the white LEDs were fabricated with an improved luminous efficiency of 81 lm W^{-1} at an injection current of 5 mA and the color coordinates of (0.32, 0.26). Huang *et al*.[83] used a layer of double-shell $MAPbBr_3/SiO_2$/PVDF NCs to fabricate WLEDs with CIE chromaticity coordinates of (0.29, 0.32), correlated color temperature (CCT) of 7968 K, a color gamut of 120% and a very high luminous efficiency of 147.5 lm W^{-1}. Favorable charge transport and better stability can be achieved with perovskite NCs capped with semiconductor shell. Zhang *et al*.[61] demonstrated that coating of $CsPbI_3$ NCs with PbS shell leads to change from n-type behavior to nearly ambipolar, The fabricated LEDs with p-i-n junctions exhibited EQE of 11.8%, and had improved storage and operational stability. Recently, the epitaxially grown $FAPbBr_3/CsPbBr_3$ NCs were also used in LED devices, and achieved enhanced EL performance with the maximum current efficiency of 19.75 cd A^{-1} and a peak EQE of 8.1% (Figure14d-e), almost 4.1-fold and 7.9-fold higher than that of the core $FAPbBr_3$-based LEDs, respectively. Moreover, the LEDs based on core/shell $FAPbBr_3/CsPbBr_3$NCs show a greatly improved operational lifetime (47 mins), which is twofold longer than those of $FAPbBr_3$-based LEDs due to the improved optical stability of

$FAPbBr_3/CsPbBr_3$NCs.[41]

5.3 Photodetectors

Large absorption coefficients, higher carrier mobility, long carrier diffusion length and long carrier lifetime[167-170] indicate tremendous prospects of perovskite NCs for applications in photodetectors. Recently, high-performance photodetectors with a layer of quasi-core/shell $CsPbBr_3$/FAI NCs were reported,[170] where the FAI salt was used to facilitate charge transfer from the core to the shell resulting in enhanced light absorption.[171] Besides, the modified inter-NCs dielectric environment as well as the surface defect passivation of NCs can also facilitate the carrier extraction and transfer in perovskite NC films. As a result, the photodetector based on quasi core/shell $CsPbBr_3$/FAI NCs exhibited dramatically enhanced detectivity of 1.7×10^{13} Jones and responsivity of 19 A W^{-1} at low applied bias of -1.5 V under illumination with 405 nm light (power density of 3 mW cm^{-2}) compared with photodetector based on $CsPbBr_3$ NCs (detectivity of 5.3×10^{11} Jones and responsivity of 7 A W^{-1}). Further enhancement of the performance of the perovskite photodetectors can be achieved by optimizing layer structure and device geometry, e.g. by combining advances in graphene-based photodetectors[172] with beneficial properties of core/shell perovskite NCs.

5.4 Lasing

$CsPbX_3$ NCs are also considered as candidate materials with great potential for two-photon-excited up-conversion devices due to the large two-photon absorption cross-section.[134, 173, 174] Li *et al.*[134] reported low threshold (P_{th}), stable random lasing with $CsPbBr_3$ NCs/aminated SiO_2 spheres. Uniform SiO_2 spheres provided strong scattering and efficient optical gain characteristics for $CsPbBr_3$ NCs, enabling lasing with a low threshold of 40 μJ cm^{-2}. High environmental and photo-stability was achieved with protection provided by the SiO_2

shell, with stable lasing intensity over optical pumping for 8 h at 1.5 times P_{th}. No measurable change of P_{th} was observed after 2 months storage in a dark drying cabinet (humidity of 30%).[175] In other work reported by Hu *et al*.,[38] non-blinking $CsPbBr_3/SiO_2$ NCs were used to obtain strong ASE. The output intensity (P_{out}) of $CsPbBr_3/SiO_2$ NCs at 1.5 times P_{th} (346 μJ cm^{-2}) is 8.8 times of the P_{out} at its P_{th}, while significantly lower value, P_{out} of 1.8 times at 1.5 times P_{th} (721 μJ cm^{-2}), was observed for core only NCs. Under the same test condition, the P_{th} of ASE reduced 50% and a 388% increase in relative efficiency was achieved (Figure 14f). The performance enhancement was attributed to an increase of the Rayleigh scattering intensity, where stronger multiple light scattering induced by the intrinsic disorder in the SiO_2 medium before light output can enhance the ASE performance.[176, 177] Moreover, a smoother surface and a large refractive index of the SiO_2 spheres facilitated total internal reflection at the SiO_2-air interface and reflect back into the disordered gain medium, hence leading to increased ASE efficiency (inset in Figure 14f). The $CsPbBr_3/SiO_2$ films retain ~ 95% of the initial PL intensity after 12 h continuous excitation with 800 nm femtosecond laser pulses (pump intensity of 600 μJ cm^{-2} in air), while the intensity of core-only $CsPbBr_3$ NCs decreased to 85%.[38]

Semiconductor coated perovskites also were investigated for ASE to achieve enhanced efficiency under both one- and two-photon excitation.[77] The P_{out} of $CsPbBr_3$/CdS NCs at 1.5 P_{th} was 3.7 times of the P_{out} at its P_{th}, while the P_{out} of the $CsPbBr_3$ NCs without CdS shell at 1.5 P_{th} only obtained 1.6 times of the P_{out} at its P_{th}, and the P_{th} of $CsPbBr_3$/CdS NCs decreased to 30 μJ cm^{-2} and relative efficiency increased by 131%. This performance enhancement was attributed to suppression of the nonradiative Auger recombination processes in the presence of CdS shell.[178] Furthermore, a high-quality factor of 1217 was achieved by incorporating $CsPbBr_3$/CdS NCs into microtubule resonators, which enhanced the total internal reflections at the interfaces between the inner tubular surfaces and the $CsPbBr_3$/CdS NCs.[77, 179]

5.5 Other applications

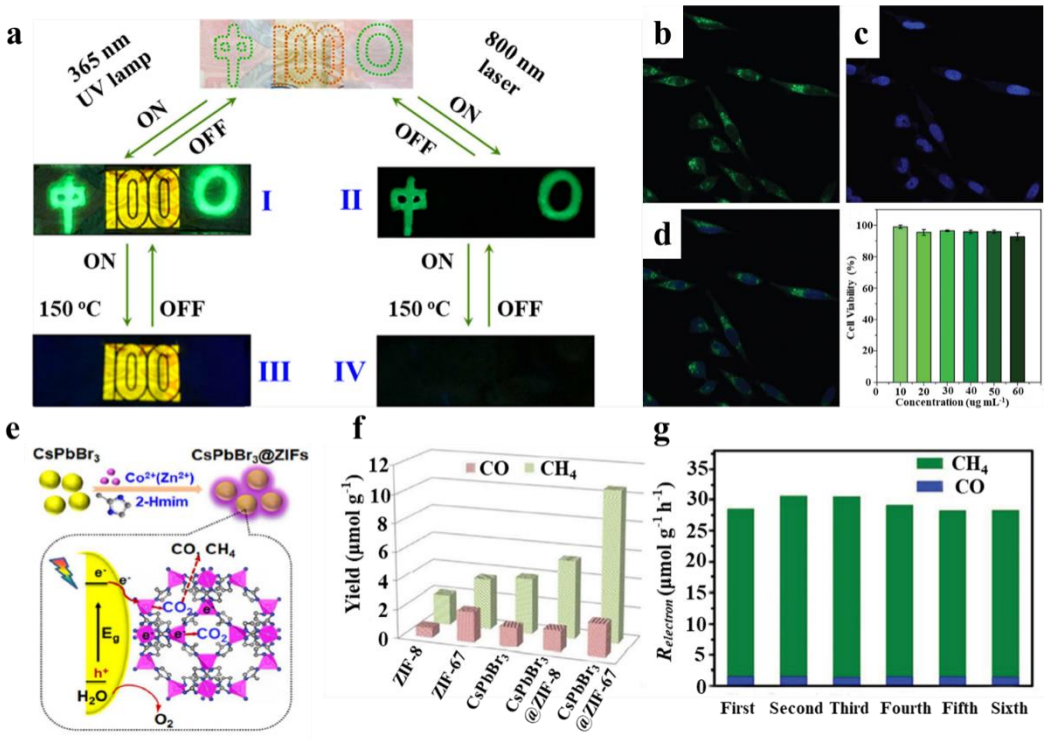

Figure 15 a) Demonstration of the triple-mode anti-counterfeiting $CsPbBr_3/Cs_4PbBr_6/SiO_2$-based films: (I, II) excitation with a 365 nm UV lamp and an 800 nm femtosecond pulse laser (turned ON) and dark (turned OFF)); (III, IV) excitation with a 365 nm UV lamp and an 800 nm femtosecond pulse laser at 150 ºC (turned OFF) and room temperature (turned ON). Reproduced with permission.[44] Copyright 2017, ACS. Confocal fluorescence microscopy images of HeLa cells after 24 h of incubation with CPB/PMMA nanospheres (20 μg mL^{-1}) and nuclei stain DAPI (1 mg mL^{-1}) with emission filtered for **b)** CPB/PMMA nanospheres, **c)** DAPI and **d)** an overlay of the two images, and cell viability of the HeLa cells upon 24 h incubation with different concentrations of CPB/PMMA nanospheres (10-60 μg mL^{-1}). Reproduced with permission.[42] Copyright 2018, Wiley-VCH. **e)** Schematic illustration of the fabrication process and CO_2 photoreduction process of $CsPbBr_3$/ZIFs. Photocatalytic CO_2 reduction performances of $CsPbBr_3$ and $CsPbBr_3$/ZIFs under AM 1.5G, 150 mW cm^{-2}: **f)** The product yield after 3 h of photocatalytic reaction. **g)** Recycling test of $CsPbBr_3$/ZIF-67 for 6 times with CO_2 refilled every 3h. Reproduced with permission.[50] Copyright 2020, ACS.

The perovskite NCs have nonlinear absorption coefficients of up to 0.085 cm/GW, and can be made stable in aqueous environment and at elevated temperatures, making them potential

interest for anti-counterfeiting applications.[44, 56, 180] Xu *et al*.[44] utilized the double-shell $CsPbBr_3/Cs_4PbBr_6/SiO_2$ perovskite NCs to prepare anti-counterfeiting inks. The designed NC ink pattern was virtually invisible in daylight and had intense green fluorescence under irradiation with the UV and IR light, which remained stable under heat treatment (T < 150 ^oC) (**Figure 15**a) and two months storage in an ambient condition.

Perovskite NCs, capped with water-soluble and non-toxic shell, also have other potential applications, such as in biomedical imaging.[42, 43, 71, 113] Wang *et al*.[42] produced $CsPbBr_3$/PMMA nanospheres with a high PLQY and good water resistance by a spray-assisted coil-globule transition method and used these core/shell NCs for live imaging of HeLa cells. The $CsPbBr_3$/PMMA nanospheres were readily uptaken by the cells with even intracellular distribution and produced high-quality fluorescence images (Figure 15b-d). Besides, the biocompatibility of $CsPbBr_3$/PMMA nanospheres was confirmed *in vitro*, with 92-99% cell survival rates of HeLa cells following exposure to the NCs at concentrations of up to 60 μg mL^{-1} (Figure 15d, right).[42] Other biocompatible core/shell perovskite NCs with good thermal and water solubility, such as $CsPbBr_3/SiO_2$[113] and $CsPbBr_3$/mPEG-NH_2,[43] were also successfully used for imaging of tumor cells and HepG2 cells. These results suggest realistic prospects for core/shell perovskite NCs, as a new generation of fluorescent probes for biomedical applications.[113, 181]

More recently, the potential application of core/shell perovskites in photocatalysis was investigated. Li *et al*.[49] coated TiO_2 shell on $CsPbBr_3$ NCs to suppress anion exchange and photodegradation, and to enhance charge separation efficiency. These NCs had significantly enhanced photoelectric activity in water, which is relevant for their application as a visible-light photocatalyst in solar energy conversion.[49] Enhanced CO_2 capturing ability was achieved by Kong *et al*.[50] for ZIF coated $CsPbBr_3$ photocatalysts, which was attributed to large specific surface area and highly active metal centers of ZIF shell (Figure 15e). The CO_2 reduction

activity with an electron consumption rate of 29.63 μmol $g^{-1}h^{-1}$ was obtained with $CsPbBr_3$/ZIF-67 photocatalyst, which is 2.6 times higher than that of core-only $CsPbBr_3$ NCs (Figure 15f). Moreover, the $CsPbBr_3$/ZIF-67 photocatalyst also showed improved stability after recycling in CO_2 refilled atmosphere every 3 h during continuous photocatalytic reaction (Figure 15g).[50]

6. Outlook

The excellent properties and extensive research on perovskite NCs, particularly recent advances in the synthesis of core/shell structure, could enable emergence of perovskite NCs and their commercialization. This paper reviewed the latest cutting-edge research and synthesis methods of metal halide perovskite NC core/shell structures. The ascension of stability and performance in core/shell perovskite NCs is emphasized, pointing out to their relevance for improved performance of solar cells, light-emitting diodes, photodetectors, cell imaging and other applications. This kind of heterostructure pushes the application of perovskite NCs to a more diversified dimension. However, as an effective means to improve the stability of heavy metal halide perovskites, the study on its core/shell heterostructure is still in its infancy, and there are some remaining challenges, which require further studies and investigations:

1. The different atomic arrangements on each surface of a cubic perovskite NC induce preferential shell growth on some surfaces, resulting in uneven shell thickness and increased lattice strain at surfaces with thicker shell layer. This may affect the properties of core/shell structure.
2. The perovskite shell has poor stability and is prone to phase transition. The decoupling caused by phase transition may have undesirable consequences, such as release of heavy metals into the environment and change of the properties of core/shell NCs.

3. Conditions used in growth of the shell often require high temperatures. Growth of covalent type shell material often needs higher temperature and longer time, and hence the development of more facile synthesis route is needed.
4. Methods for up-scalable growth of core/shell structures with even thickness and monodisperse size distribution should be explored.
5. Perovskite derivatives and some traditional semiconductors used as shell materials also contain heavy metals, which has not only environmental implications, but also could limit their potential for applications (e.g. bioimaging).

In summary, the future research direction is to choose the environmentally friendly shell materials for perovskite NCs and to develop more effective coating strategies to produce high-quality core/shell structures, improved environmental stability of perovskite, while achieving enhanced performance in optoelectronic devices and other applications.

Acknowledgements

C. Z. and J. C. contributed equally to this work. We acknowledge financial support from the Australian Research Council (ARC) Discovery Early Career Researcher Award (DE160100589), National Natural Science Foundation of China (61735004 and 51675322), National Key Research and Development Program of China (2016YFB0401702), Shanghai Science and Technology Committee (19010500600) and China Postdoctoral Science Foundation (2020M680054). L. T. acknowledges support from the Engineering and Physical Sciences Research Council (EP/P031684/1).

Conflict of Interest

The authors declare no conflict of interest.

Received: ((will be filled in by the editorial staff))

Revised: ((will be filled in by the editorial staff))

Published online: ((will be filled in by the editorial staff))

References:

[1] V. K. Ravi, A. Swarnkar, R. Chakraborty, A. Nag, *Nanotechnology* **2016**, 27, 325708.

[2] J. Maes, L. Balcaen, E. Drijvers, Q. Zhao, J. De Roo, A. Vantomme, F. Vanhaecke, P. Geiregat, Z. Hens, *J. Phys. Chem. Lett.* **2018**, 9, 3093.

[3] J. De Roo, M. Ibáñez, P. Geiregat, G. Nedelcu, W. Walravens, J. Maes, J. C. Martins, I. Van Driessche, M. V. Kovalenko, Z. Hens, *ACS Nano* **2016**, 10, 2071.

[4] C. Zhang, J. Chen, S. Wang, L. Kong, S. W. Lewis, X. Yang, A. L. Rogach, G. Jia, *Adv. Mater.* **2020**, 32, 2002736.

[5] J. Li, L. Xu, T. Wang, J. Song, J. Chen, J. Xue, Y. Dong, B. Cai, Q. Shan, B. Han, *Adv. Mater.* **2017**, 29, 1603885.

[6] C. Zhang, L. Turyanska, H. Cao, L. Zhao, M. W. Fay, R. Temperton, J. O'Shea, N. R. Thomas, K. Wang, W. Luan, A. Patanè, *Nanoscale* **2019**, 11, 13450.

[7] H. Wang, X. Gong, D. Zhao, Y.-B. Zhao, S. Wang, J. Zhang, L. Kong, B. Wei, R. Quintero-Bermudez, O. Voznyy, Y. Shang, Z. Ning, Y. Yan, E. H. Sargent, X. Yang, *Joule* **2020**, 4, 1977.

[8] S. Yakunin, L. Protesescu, F. Krieg, M. I. Bodnarchuk, G. Nedelcu, M. Humer, G. De Luca, M. Fiebig, W. Heiss, M. V. Kovalenko, *Nat. Commun.* **2015**, 6, 1.

[9] Y. Dou, F. Cao, T. Dudka, Y. Li, S. Wang, C. Zhang, Y. Gao, X. Yang, A. L. Rogach, *ACS Mater. Lett.* **2020**, 2, 814.

[10] P. Ramasamy, D.-H. Lim, B. Kim, S.-H. Lee, M.-S. Lee, J.-S. Lee, *Chem. Commun.* **2016**, 52, 2067.

[11] H. Zhang, X. Wang, Q. Liao, Z. Xu, H. Li, L. Zheng, H. Fu, *Adv. Funct. Mater.* **2017**, 27, 1604382.

[12] J.-H. Im, C.-R. Lee, J.-W. Lee, S.-W. Park, N.-G. Park, *Nanoscale* **2011**, 3, 4088.

[13] X. Zhu, Y. Lin, J. San Martin, Y. Sun, D. Zhu, Y. Yan, *Nat. Commun.* **2019**, 10, 1.

[14] C. C. Stoumpos, M. G. Kanatzidis, *Accounts Chem. Res.* **2015**, 48, 2791.

[15] C. Liu, Q. Zeng, H. Wei, Y. Yu, Y. Zhao, T. Feng, B. Yang, *Small Methods* **2020**, 4, 2000419.

[16] A. Toshniwal, V. Kheraj, *Sol. Energy* **2017**, 149, 54.

[17] W. Xiang, W. Tress, *Adv. Mater.* **2019**, 31, 1902851.

[18] R. Shwetharani, V. Nayak, M. Jyothi, R. G. Balakrishna, *J. Alloys Compd.* **2020**, 155246.

[19] Y. Huang, W. Luan, M. Liu, L. Turyanska, *J. Mater. Chem. C* **2020**, 8, 2381.

[20] J. Song, T. Fang, J. Li, L. Xu, F. Zhang, B. Han, Q. Shan, H. Zeng, *Adv. Mater.* **2018**, 30, 1805409.

[21] L. Wu, Q. Zhong, D. Yang, M. Chen, H. Hu, Q. Pan, H. Liu, M. Cao, Y. Xu, B. Sun, Q. Zhang, *Langmuir* **2017**, 33, 12689.

[22] B. Mahler, B. Nadal, C. Bouet, G. Patriarche, B. Dubertret, *J. Am. Chem. Soc.* **2012**, 134, 18591.

[23] R. Xie, M. Rutherford, X. Peng, *J. Am. Chem. Soc.* **2009**, 131, 5691.

[24] D. Chen, A. Wang, H. Li, L. A. Galán, C. Su, Z. Yin, M. Massi, A. Suvorova, M. Saunders, J. Li, *Nanoscale* **2019**, 11, 10190.

[25] O. Chen, J. Zhao, V. P. Chauhan, J. Cui, C. Wong, D. K. Harris, H. Wei, H.-S. Han, D. Fukumura, R. K. Jain, *Nat. Mater.* **2013**, 12, 445.

[26] H. Yang, W. Luan, Z. Wan, S.-t. Tu, W.-K. Yuan, Z. M. Wang, *Cryst. Growth Des.* **2009**, 9, 4807.

[27] Z. Wan, W. Luan, S.-t. Tu, *J. Phys. Chem. C* **2011**, 115, 1569.

[28] P. Reiss, M. Protiere, L. Li, *small* **2009**, 5, 154.

[29] R. Ghosh Chaudhuri, S. Paria, *Chem. Rev.* **2012**, 112, 2373.

[30] M. V. Kovalenko, L. Protesescu, M. I. Bodnarchuk, *Science* **2017**, 358, 745.

[31] B. Qiao, P. Song, J. Cao, S. Zhao, Z. Shen, G. Di, Z. Liang, Z. Xu, D. Song, X. Xu, *Nanotechnology* **2017**, 28, 445602.

[32] Y. Pang, M. N. Uddin, W. Chen, S. Javaid, E. Barker, Y. Li, A. Suvorova, M. Saunders, Z. Yin, G. Jia, *Adv. Mater.* **2019**, 31, 1905540.

[33] D. Chen, H. Zhang, Y. Li, Y. Pang, Z. Yin, H. Sun, L.-C. Zhang, S. Wang, M. Saunders, E. Barker, G. Jia, *Adv. Mater.* **2018**, 30, 1803351.

[34] T. Yang, Y. Zheng, Z. Du, W. Liu, Z. Yang, F. Gao, L. Wang, K. C. Chou, X. Hou, W. Yang, *ACS Nano* **2018**, 12, 1611.

[35] C. Bi, S. Kershaw, A. Rogach, J. Tian, *Adv. Funct. Mater.* **2019**, 29.

[36] Y. Cao, N. Wang, H. Tian, J. Guo, Y. Wei, H. Chen, Y. Miao, W. Zou, K. Pan, Y. He, H. Cao, Y. Ke, M. Xu, Y. Wang, M. Yang, K. Du, Z. Fu, D. Kong, D. Dai, Y. Jin, G. Li, H. Li, Q. Peng, J. Wang, W. Huang, *Nature* **2018**, 562, 249.

[37] C. Jia, H. Li, X. Meng, H. Li, *Chem. Commun.* **2018**, 54, 6300.

[38] Z. Hu, Z. Liu, Y. Bian, S. Li, X. Tang, J. Du, Z. Zang, M. Zhou, W. Hu, Y. Tian, Y. Leng, *Adv. Opt. Mater.* **2018**, 6, 1700997.

[39] W. Yang, F. Gao, Y. Qiu, W. Liu, H. Xu, L. Yang, Y. Liu, *Adv. Opt. Mater.* **2019**, 7, 1900546.

[40] W. Chen, J. Hao, W. Hu, Z. Zang, X. Tang, L. Fang, T. Niu, M. Zhou, *Small* **2017**, 13, 1604085.

[41] C. Zhang, S. Wang, X. Li, M. Yuan, L. Turyanska, X. Yang, *Adv. Funct. Mater.* **2020**, 30, 1910582.

[42] Y. Wang, L. Varadi, A. Trinchi, J. Shen, Y. Zhu, G. Wei, C. Li, *Small* **2018**, 14, 1803156.

[43] Q.-B. Yan, N. Bao, S.-N. Ding, *J. Mater. Chem. B* **2019**, 7, 4153.

[44] L. Xu, J. Chen, J. Song, J. Li, J. Xue, Y. Dong, B. Cai, Q. Shan, B. Han, H. Zeng, *ACS Appl. Mater. Inter.* **2017**, 9, 26556.

[45] Junwei Xu, Wenxiao Huang, Peiyun Li, Drew R. Onken, Chaochao Dun, Yang Guo, Kamil B. Ucer, Chang Lu, Hongzhi Wang, Scott M. Geyer, Richard T. Williams, D. L. Carroll, *Adv. Mater.* **2017**, 29, 1703703.

[46] B. Wang, C. Zhang, S. Huang, Z. Li, L. Kong, L. Jin, J. Wang, K. Wu, L. Li, *ACS Appl. Mater. Inter.* **2018**, 10, 23303.

[47] X. Tang, J. Yang, S. Li, W. Chen, Z. Hu, J. Qiu, *Front. Chem.* **2019**, 7, 499.

[48] Y. Wang, Q. Wang, X. Zhan, F. Wang, M. Safdar, J. He, *Nanoscale* **2013**, 5, 8326.

[49] Z.-J. Li, E. Hofman, J. Li, A. H. Davis, C.-H. Tung, L.-Z. Wu, W. Zheng, *Adv. Funct. Mater.* **2018**, 28, 1704288.

[50] Z.-C. Kong, J.-F. Liao, Y.-J. Dong, Y.-F. Xu, H.-Y. Chen, D.-B. Kuang, C.-Y. Su, *ACS Energy Lett.* **2018**, 3, 2656.

[51] H. Liu, Y. Tan, M. Cao, H. Hu, L. Wu, X. Yu, L. Wang, B. Sun, Q. Zhang, *ACS Nano* **2019**, 13, 5366.

[52] G. Kaur, K. Justice Babu, N. Ghorai, T. Goswami, S. Maiti, H. N. Ghosh, *J. Phys. Chem. Lett.* **2019**, 10, 5302.

[53] V. K. Ravi, S. Saikia, S. Yadav, V. V. Nawale, A. Nag, *ACS Energy Lett.* **2020**, 5, 1794.

[54] L. Li, T. J. Daou, I. Texier, T. T. Kim Chi, N. Q. Liem, P. Reiss, *Chem. Mater.* **2009**, 21, 2422.

[55] B. N. Pal, Y. Ghosh, S. Brovelli, R. Laocharoensuk, V. I. Klimov, J. A. Hollingsworth, H. Htoon, *Nano Lett.* **2012**, 12, 331.

[56] D. Poirot, R. Platel, T. Alnasser, F. Guerin, E. Palleau, L. Ressier, *ACS Appl. Nano Mater.* **2018**, 1, 5936.

[57] J. Wang, I. Mora-Seró, Z. Pan, K. Zhao, H. Zhang, Y. Feng, G. Yang, X. Zhong, J. Bisquert, *J. Am. Chem. Soc.* **2013**, 135, 15913.

[58] J. Bang, J. Park, J. H. Lee, N. Won, J. Nam, J. Lim, B. Y. Chang, H. J. Lee, B. Chon, J. Shin, *Chem. Mater.* **2010**, 22, 233.

[59] S. Kumar, S. Khanchandani, M. Thirumal, A. K. Ganguli, *ACS Appl. Mater. Inter.* **2014**, 6, 13221.

[60] P. Reiss, S. Carayon, J. Bleuse, A. Pron, *Synth. Met.* **2003**, 139, 649.

[61] X. Zhang, M. Lu, Y. Zhang, H. Wu, X. Shen, W. Zhang, W. Zheng, V. L. Colvin, W. W. Yu, *ACS Cent. Sci.* **2018**, 4, 1352.

[62] C. Tan, J. Chen, X.-J. Wu, H. Zhang, *Nat. Rev. Mater.* **2018**, 3, 17089.

[63] F.-R. Fan, D.-Y. Liu, Y.-F. Wu, S. Duan, Z.-X. Xie, Z.-Y. Jiang, Z.-Q. Tian, *J. Am. Chem. Soc.* **2008**, 130, 6949.

[64] S. Yang, D. Prendergast, J. B. Neaton, *Nano Lett.* **2010**, 10, 3156.

[65] M. Jin, H. Zhang, J. Wang, X. Zhong, N. Lu, Z. Li, Z. Xie, M. J. Kim, Y. Xia, *ACS nano* **2012**, 6, 2566.

[66] Y. Jang, A. Shapiro, M. Isarov, A. Rubin-Brusilovski, A. Safran, A. K. Budniak, F. Horani, J. Dehnel, A. Sashchiuk, E. Lifshitz, *Chem. Commun.* **2017**, 53, 1002.

[67] J. Van Embden, J. Jasieniak, D. E. Gómez, P. Mulvaney, M. Giersig, *Aust. J. Chem.* **2007**, 60, 457.

[68] A. M. Smith, A. M. Mohs, S. Nie, *Nat. Nanotechnol.* **2009**, 4, 56.

[69] W. Chen, S. Bhaumik, S. A. Veldhuis, G. Xing, Q. Xu, M. Gratzel, S. Mhaisalkar, N. Mathews, T. C. Sum, *Nat. Commun.* **2017**, 8, 15198.

[70] Q. A. Akkerman, G. Rainò, M. V. Kovalenko, L. Manna, *Nat. Mater.* **2018**, 17, 394.

[71] A. Pramanik, K. Gates, S. Patibandla, D. Davis, S. Begum, R. Iftekhar, S. Alamgir, S. Paige, M. M. Porter, P. C. Ray, *ACS Appl. Bio Mater.* **2019**, 2, 5872.

[72] W. Li, C. Zhang, Y. Ma, C. Liu, J. Fan, Y. Mai, R. E. I. Schropp, *Energy Environ. Sci.* **2018**, 11, 286.

[73] G. Zhang, P. Song, Z. Shen, B. Qiao, D. Song, J. Cao, Z. Xu, W. Swelm, A. Al-Ghamdi, S. Zhao, *ACS Omega* **2020**, 5, 11578.

[74] S. Wang, C. Bi, J. Yuan, L. Zhang, J. Tian, *ACS Energy Lett.* **2017**, 3, 245.

[75] S. Bhaumik, S. A. Veldhuis, Y. F. Ng, M. Li, S. K. Muduli, T. C. Sum, B. Damodaran, S. Mhaisalkar, N. Mathews, *Chem. Commun.* **2016**, 52, 7118.

[76] C. V. Mary Vijila, K. Rajeev Kumar, M. K. Jayaraj, *Opt. Mater.* **2019**, 94, 241.

[77] X. Tang, J. Yang, S. Li, Z. Liu, Z. Hu, J. Hao, J. Du, Y. Leng, H. Qin, X. Lin, Y. Lin, Y. Tian, M. Zhou, Q. Xiong, *Adv. Sci.* **2019**, 6, 1900412.

[78] X. Liu, X. Zhang, L. Li, J. Xu, S. Yu, X. Gong, J. Zhang, H. Yin, *ACS Appl. Mater. Inter.* **2019**, 11, 40923.

[79] X. Tang, W. Chen, Z. Liu, J. Du, Z. Yao, Y. Huang, C. Chen, Z. Yang, T. Shi, W. Hu, Z. Zang, Y. Chen, Y. Leng, *Small* **2019**, 15, 1900484.

[80] C. Sun, Y. Zhang, C. Ruan, C. Yin, X. Wang, Y. Wang, W. W. Yu, *Adv. Mater.* **2016**, 28, 10088.

[81] T. Song, X. Feng, H. Ju, T. Fang, F. Zhu, W. Liu, W. Huang, *J. Alloys Compd.* **2020**, 816, 152558.

[82] S. M. Lee, H. Jung, W. I. Park, Y. Lee, E. Koo, J. Bang, *ChemistrySelect* **2018**, 3, 11320.

[83] Y. Huang, F. Li, L. Qiu, F. Lin, Z. Lai, S. Wang, L. Lin, Y. Zhu, Y. Wang, Y. Jiang, X. Chen, *ACS Appl. Mater. Inter.* **2019**, 11, 26384.

[84] Z. Li, L. Kong, S. Huang, L. Li, *Angew. Chem. Int. Ed.* **2017**, 56, 8134.

[85] H. Hu, L. Wu, Y. Tan, Q. Zhong, M. Chen, Y. Qiu, D. Yang, B. Sun, Q. Zhang, Y. Yin, *J. Am. Chem. Soc.* **2018**, 140, 406.

[86] Y. Ye, W. Zhang, Z. Zhao, J. Wang, C. Liu, Z. Deng, X. Zhao, J. Han, *Adv. Opt. Mater.* **2019**, 7, 1801663.

[87] Y. Li, H. Huang, Y. Xiong, A. F. Richter, S. V. Kershaw, J. Feldmann, A. L. Rogach, *ACS Nano* **2019**, 13, 8237.

[88] A. B. Wong, M. Lai, S. W. Eaton, Y. Yu, E. Lin, L. Dou, A. Fu, P. Yang, *Nano Lett.* **2015**, 15, 5519.

[89] F. Cao, D. Yu, Y. Gu, J. Chen, H. Zeng, *Nanoscale* **2019**, 11, 3117.

[90] K. Xu, C. C. Lin, X. Xie, A. Meijerink, *Chem. Mater.* **2017**, 29, 4265.

[91] R. Martín-Rodríguez, R. Geitenbeek, A. Meijerink, *J. Am. Chem. Soc.* **2013**, 135, 13668.

[92] Y. Zhao, F. T. Rabouw, T. v. Puffelen, C. A. v. Walree, D. R. Gamelin, C. de Mello Donegá, A. Meijerink, *J. Am. Chem. Soc.* **2014**, 136, 16533.

[93] J. F. Suyver, J. J. Kelly, A. Meijerink, *J. Lumin.* **2003**, 104, 187.

[94] J. Tian, G. Cao, *Coord. Chem. Rev.* **2016**, 320-321, 193.

[95] Q. Wang, W. Wu, R. Wu, S. Yang, Y. Wang, J. Wang, Z. Chai, Q. Han, *J. Colloid Interface Sci.* **2019**, 554, 133.

[96] J. Shi, W. Ge, J. Zhu, M. Saruyama, T. Teranishi, *ACS Appl. Nano Mater.* **2020**, 3, 7563.

[97] J. M. Pietryga, D. J. Werder, D. J. Williams, J. L. Casson, R. D. Schaller, V. I. Klimov, J. A. Hollingsworth, *J. Am. Chem. Soc.* **2008**, 130, 4879.

[98] C. S. Erickson, L. R. Bradshaw, S. McDowall, J. D. Gilbertson, D. R. Gamelin, D. L. Patrick, *ACS Nano* **2014**, 8, 3461.

[99] T. P. Nguyen, A. Ozturk, J. Park, W. Sohn, T. H. Lee, H. W. Jang, S. Y. Kim, *Sci. Technol. Adv. Mater.* **2018**, 19, 10.

[100] G. Jia, A. Sitt, G. B. Hitin, I. Hadar, Y. Bekenstein, Y. Amit, I. Popov, U. Banin, *Nat. Mater.* **2014**, 13, 301.

[101] R. K. Ratnesh, M. S. Mehata, *Spectrochim. Acta A Mol. Biomol. Spectrosc.* **2017**, 179, 201.

[102] D. Saikia, S. Chakravarty, N. S. Sarma, S. Bhattacharjee, P. Datta, N. C. Adhikary, *Luminescence* **2017**, 32, 401.

[103] L. Li, A. Pandey, D. J. Werder, B. P. Khanal, J. M. Pietryga, V. I. Klimov, *J. Am. Chem. Soc.* **2011**, 133, 1176.

[104] J. Kwak, J. Lim, M. Park, S. Lee, K. Char, C. Lee, *Nano Lett.* **2015**, 15, 3793.

[105] U. Soni, S. Sapra, *J. Phys. Chem. C* **2010**, 114, 22514.

[106] X. Gong, Z. Yang, G. Walters, R. Comin, Z. Ning, E. Beauregard, V. Adinolfi, O. Voznyy, E. H. Sargent, *Nat. Photonics* **2016**, 10, 253.

[107] J. R. Dethlefsen, A. Døssing, *Nano Lett.* **2011**, 11, 1964.

[108] Q. Zhong, M. Cao, H. Hu, D. Yang, M. Chen, P. Li, L. Wu, Q. Zhang, *ACS Nano* **2018**, 12, 8579.

[109] J. Cai, K. Gu, Y. Zhu, J. Zhu, Y. Wang, J. Shen, A. Trinchi, C. Li, G. Wei, *Chem. Commun.* **2018**, 54, 8064.

[110] D. H. Park, J. S. Han, W. Kim, H. S. Jang, *Dyes Pigm.* **2018**, 149, 246.

[111] P. Cao, B. Yang, Y. Geng, Y. Cao, L. Wang, F. Zheng, J. Zou, *ECS J. Solid State Sci. Technol.* **2020**, 9, 046001.

[112] P. Cao, B. Yang, F. Zheng, L. Wang, J. Zou, *Ceram. Int.* **2020**, 46, 3882.

[113] W. Song, Y. Wang, B. Wang, Y. Yao, W. Wang, J. Wu, Q. Shen, W. Luo, Z. Zou, *Nano Res.* **2020**, 13, 795.

[114] B. Wang, S. Zhang, B. Liu, J. Li, B. Cao, Z. Liu, *ACS Appl. Nano Mater.* **2020**, 3, 3019.

[115] C. Zhang, H. Zhang, R. Wang, D. You, W. Wang, C. Xu, J. Dai, *Opt. Mater. Express* **2020**, 10, 1007.

[116] Q. Zhang, B. Wang, W. Zheng, L. Kong, Q. Wan, C. Zhang, Z. Li, X. Cao, M. Liu, L. Li, *Nat. Commun.* **2020**, 11, 31.

[117] L. Zhou, K. Yu, F. Yang, H. Cong, N. Wang, J. Zheng, Y. Zuo, C. Li, B. Cheng, Q. Wang, *J. Mater. Chem. C* **2017**, 5, 6224.

[118] A. Loiudice, S. Saris, E. Oveisi, D. T. L. Alexander, R. Buonsanti, *Angew. Chem. Int. Ed.* **2017**, 56, 10696.

[119] F. Zhang, H. Zhong, C. Chen, X.-g. Wu, X. Hu, H. Huang, J. Han, B. Zou, Y. Dong, *ACS Nano* **2015**, 9, 4533.

[120] D. Yang, M. Cao, Q. Zhong, P. Li, X. Zhang, Q. Zhang, *J. Mater. Chem. C* **2019**, 7, 757.

[121] L. Wu, H. Hu, Y. Xu, S. Jiang, M. Chen, Q. Zhong, D. Yang, Q. Liu, Y. Zhao, B. Sun, Q. Zhang, Y. Yin, *Nano Lett.* **2017**, 17, 5799.

[122] D. Yang, P. Li, Y. Zou, M. Cao, H. Hu, Q. Zhong, J. Hu, B. Sun, S. Duhm, Y. Xu, Q. Zhang, *Chem. Mater.* **2019**, 31, 1575.

[123] W. C. Liu, B. L. Guo, X. S. Wu, F. M. Zhang, C. L. Mak, K. H. Wong, *J. Mater. Chem. A* **2013**, 1, 3182.

[124] Y. Chen, L. Ma, Y. Yin, X. Qian, G. Zhou, X. Gu, W. Liu, X. Wu, F. Zhang, *J. Alloys Compd.* **2016**, 672, 204.

[125] X. Chen, S. S. Mao, *Chem. Rev.* **2007**, 107, 2891.

[126] J. Yu, Y. Su, B. Cheng, M. Zhou, *J. Mol. Catal. A Chem.* **2006**, 258, 104.

[127] Y. Xia, X. Xia, H.-C. Peng, *J. Am. Chem. Soc.* **2015**, 137, 7947.

[128] C. Noda Pérez, E. Moreno, C. A. Henriques, S. Valange, Z. Gabelica, J. L. F. Monteiro, *Microporous Mesoporous Mater.* **2000**, 41, 137.

[129] G. Li, Z. K. Tan, D. Di, M. L. Lai, L. Jiang, J. H. Lim, R. H. Friend, N. C. Greenham, *Nano Lett.* **2015**, 15, 2640.

[130] P. C. Tsai, J. Y. Chen, E. Ercan, C. C. Chueh, S. H. Tung, W. C. Chen, *Small* **2018**, 14, 1704379.

[131] D. Di, K. P. Musselman, G. Li, A. Sadhanala, Y. Ievskaya, Q. Song, Z. K. Tan, M. L. Lai, J. L. MacManus-Driscoll, N. C. Greenham, R. H. Friend, *J. Phys. Chem. Lett.* **2015**, 6, 446.

[132] Q. Zhou, Z. Bai, W. G. Lu, Y. Wang, B. Zou, H. Zhong, *Adv. Mater.* **2016**, 28, 9163.

[133] X. Gao, Y. Cui, R. M. Levenson, L. W. K. Chung, S. Nie, *Nat. Biotechnol.* **2004**, 22, 969.

[134] X. Li, Y. Wang, H. Sun, H. Zeng, *Adv. Mater.* **2017**, 29, 1701185.

[135] V. Malgras, S. Tominaka, J. W. Ryan, J. Henzie, T. Takei, K. Ohara, Y. Yamauchi, *J. Am. Chem. Soc.* **2016**, 138, 13874.

[136] D. N. Dirin, L. Protesescu, D. Trummer, I. V. Kochetygov, S. Yakunin, F. Krumeich, N. P. Stadie, M. V. Kovalenko, *Nano Lett.* **2016**, 16, 5866.

[137] A. Lemaire, J. C. Rooke, L.-H. Chen, B.-L. Su, *Langmuir* **2011**, 27, 3030.

[138] J. Y. Woo, J.-H. Ko, J. H. Song, K. Kim, H. Choi, Y.-H. Kim, D. C. Lee, S. Jeong, *J. Am. Chem. Soc.* **2014**, 136, 8883.

[139] Y.-T. Lin, C.-H. Hsieh, S.-Y. Chu, *Ceram. Int.* **2020**, 46, 11563.

[140] L. Huang, T. Liao, J. Wang, L. Ao, W. Su, J. Hu, *Adv. Funct. Mater.* **2018**, 28, 1705380.

[141] H. Donya, T. A. Taha, *J. Mater. Sci. Mater. Electron.* **2018**, 29, 8610.

[142] M. Xia, C. Liu, Y. Xu, X. Zhao, *J. Am. Ceram. Soc.* **2019**, 102, 1726.

[143] M. Xia, C. Liu, Z. Zhao, J. Wang, C. Lin, Y. Xu, J. Heo, S. Dai, J. Han, X. Zhao, *Sci. Rep.* **2017**, 7, 42359.

[144] X. Di, Z. Hu, J. Jiang, M. He, L. Zhou, W. Xiang, X. Liang, *Chem. Commun.* **2017**, 53, 11068.

[145] R. Yuan, L. Shen, C. Shen, J. Liu, L. Zhou, W. Xiang, X. Liang, *Chem. Commun.* **2018**, 54, 3395.

[146] B. Ai, C. Liu, J. Wang, J. Xie, J. Han, X. Zhao, *J. Am. Ceram. Soc.* **2016**, 99, 2875.

[147] S. Liu, Y. Luo, M. He, X. Liang, W. Xiang, *J. Am. Ceram. Soc.* **2018**, 38, 1998.

[148] P. Li, C. Hu, L. Zhou, J. Jiang, Y. Cheng, M. He, X. Liang, W. Xiang, *Mater. Lett.* **2017**, 209, 483.

[149] C. Wang, H. Lin, Z. Zhang, Z. Qiu, H. Yang, Y. Cheng, J. Xu, X. Xiang, L. Zhang, Y. Wang, *J. Am. Ceram. Soc.* **2020**, 40, 2234.

[150] S. Yuan, D. Chen, X. Li, J. Zhong, X. Xu, *ACS Appl. Mater. Inter.* **2018**, 10, 18918.

[151] D. Chen, S. Yuan, J. Chen, J. Zhong, X. Xu, *J. Mater. Chem. C* **2018**, 6, 12864.

[152] D. Chen, S. Yuan, X. Chen, J. Li, Q. Mao, X. Li, J. Zhong, *J. Mater. Chem. C* **2018**, 6, 6832.

[153] I. Pelant, J. Valenta, *Luminescence spectroscopy of semiconductors*, Oxford University Press, **2012**.

[154] H. C. Yoon, S. Lee, J. K. Song, H. Yang, Y. R. Do, *ACS Appl. Mater. Inter.* **2018**, 10, 11756.

[155] H. C. Yoon, H. Lee, H. Kang, J. H. Oh, Y. R. Do, *J. Mater. Chem. C* **2018**, 6, 13023.

[156] G. Yang, Q. Fan, B. Chen, Q. Zhou, H. Zhong, *J. Mater. Chem. C* **2016**, 4, 11387.

[157] M. J. Ashley, E. J. Kluender, C. A. Mirkin, *ACS Nano* **2018**, 12, 7206.

[158] S. D. Stranks, G. E. Eperon, G. Grancini, C. Menelaou, M. J. Alcocer, T. Leijtens, L. M. Herz, A. Petrozza, H. J. Snaith, *Science* **2013**, 342, 341.

[159] G. Xing, N. Mathews, S. Sun, S. S. Lim, Y. M. Lam, M. Grätzel, S. Mhaisalkar, T. C. Sum, *Science* **2013**, 342, 344.

[160] Z. Xiao, R. A. Kerner, L. Zhao, N. L. Tran, K. M. Lee, T.-W. Koh, G. D. Scholes, B. P. Rand, *Nat. Photonics* **2017**, 11, 108.

[161] V. Biju, R. Kanemoto, Y. Matsumoto, S. Ishii, S. Nakanishi, T. Itoh, Y. Baba, M. Ishikawa, *J. Phys. Chem. C* **2007**, 111, 7924.

[162] M. Ikeguchi, S. Shimizu, S. Nakamura, K. Shimizu, *J. Phys. Chem. B* **1998**, 102, 5891.

[163] F. Fang, W. Chen, Y. Li, H. Liu, M. Mei, R. Zhang, J. Hao, M. Mikita, W. Cao, R. Pan, K. Wang, X. W. Sun, *Adv. Funct. Mater.* **2018**, 28, 1706000.

[164] X. Zhang, X. Bai, H. Wu, X. Zhang, C. Sun, Y. Zhang, W. Zhang, W. Zheng, W. W. Yu, A. L. Rogach, *Angew. Chem. Int. Ed.* **2018**, 57, 3337.

[165] https://www.nrel.gov/pv/cell-efficiency.html.

[166] Y.-T. Lin, C.-H. Huang, C.-H. Hsieh, S.-Y. Chu, *IEEE Trans. Electron Devices* **2020**, 67, 2386.

[167] L. Yan, Q. Xue, M. Liu, Z. Zhu, J. Tian, Z. Li, Z. Chen, Z. Chen, H. Yan, H.-L. Yip, Y. Cao, *Adv. Mater.* **2018**, 30, 1802509.

[168] W. S. Yang, B.-W. Park, E. H. Jung, N. J. Jeon, Y. C. Kim, D. U. Lee, S. S. Shin, J. Seo, E. K. Kim, J. H. Noh, S. I. Seok, *Science* **2017**, 356, 1376.

[169] Z. Yang, Q. Xu, X. Wang, J. Lu, H. Wang, F. Li, L. Zhang, G. Hu, C. Pan, *Adv. Mater.* **2018**, 30, 1802110.

[170] M. I. Saleem, S. Yang, R. Zhi, M. Sulaman, P. V. Chandrasekar, Y. Jiang, Y. Tang, A. Batool, B. Zou, *Adv. Mater. Interfaces* **2020**, 7, 2000360.

[171] K. T. Cho, S. Paek, G. Grancini, C. Roldán-Carmona, P. Gao, Y. Lee, M. K. Nazeeruddin, *Energy Environ. Sci.* **2017**, 10, 621.

[172] N. D. Cottam, C. Zhang, L. Turyanska, L. Eaves, Z. Kudrynskyi, E. E. Vdovin, A. Patanè, O. Makarovsky, *ACS Appl. Electron. Mater.* **2020**, 2, 147.

[173] X. Tang, Z. Hu, W. Yuan, W. Hu, H. Shao, D. Han, J. Zheng, J. Hao, Z. Zang, J. Du, Y. Leng, L. Fang, M. Zhou, *Adv. Opt. Mater.* **2017**, 5, 1600788.

[174] S. Wang, J. Yu, M. Zhang, D. Chen, C. Li, R. Chen, G. Jia, A. L. Rogach, X. Yang, *Nano Lett.* **2019**, 19, 6315.

[175] S. Gottardo, R. Sapienza, P. D. García, A. Blanco, D. S. Wiersma, C. López, *Nat. Photonics* **2008**, 2, 429.

[176] D. Wiersma, *Nature* **2000**, 406, 133.

[177] D. S. Wiersma, *Nat. Phys.* **2008**, 4, 359.

[178] A. Jain, O. Voznyy, M. Korkusinski, P. Hawrylak, E. H. Sargent, *J. Phys. Chem. Lett.* **2017**, 8, 3179.

[179] Y. Xu, Q. Chen, C. Zhang, R. Wang, H. Wu, X. Zhang, G. Xing, W. W. Yu, X. Wang, Y. Zhang, M. Xiao, *J. Am. Chem. Soc.* **2016**, 138, 3761.

[180] G. Gao, D. Busko, R. Joseph, I. A. Howard, A. Turshatov, B. S. Richards, *ACS Appl. Mater. Inter.* **2018**, 10, 39851.

[181] J. Sanz, Z. A. Fayad, *Nature* **2008**, 451, 953.

Author Biography

Guohua Jia is a senior lecturer and senior research fellow in the School of Molecular and Life Science at Curtin University, Australia. He obtained his PhD degree in chemistry in 2009 from City University of Hong Kong. He was a postdoctoral fellow at the Hebrew University of Jerusalem in Israel from 2010 to 2014 prior to his current appointment. His research interests focus on chemistry and physics of colloidal NCs, with particular emphasis on their shape-dependent properties and applications in optoelectronic devices and catalysis.

Author Biography

Xuyong Yang is a Full Professor ("Eastern Scholar") in the Key Laboratory of Advanced Display and System Applications of Ministry of Education in Shanghai University, China. He received his PhD degree in microelectronics from Nanyang Technological University in Singapore in 2014, and worked as a postdoc at the same university prior to beginning his independent research career at Shanghai University. His research focuses primarily on design

and fabrication of low dimensional luminescent nanomaterials such as quantum dots and nanorods, as well as their applications in various optoelectronic devices.

Core/shell metal halide perovskite nanocrystals show enhanced stability and optical properties, which are beneficial for their applications in lighting and displays, solar cells, photodetectors, lasing, photocatalysis and biomedical imaging. In this review, recent advances in synthetic strategies and shell growth of core/shell nanocrystals are reviewed, and their enhanced material properties and emerging applications are discussed.

Keywords: metal halide perovskites, core/shell nanocrystals, shell growth mechanisms, optical properties, optoelectronics

C Zhang, J. Chen, L. Kong, L. Wang, S. Wang, W. Chen, R. Mao, L. Turyanska, G. Jia and X. Yang**

Core/Shell Metal Halide Perovskite Nanocrystals for Optoelectronic Applications

TOC Figure